Article

Cell Reports

Selective Vulnerability of Cancer Cells by Inhibition of Ca^{2+} Transfer from Endoplasmic Reticulum to Mitochondria

Graphical Abstract

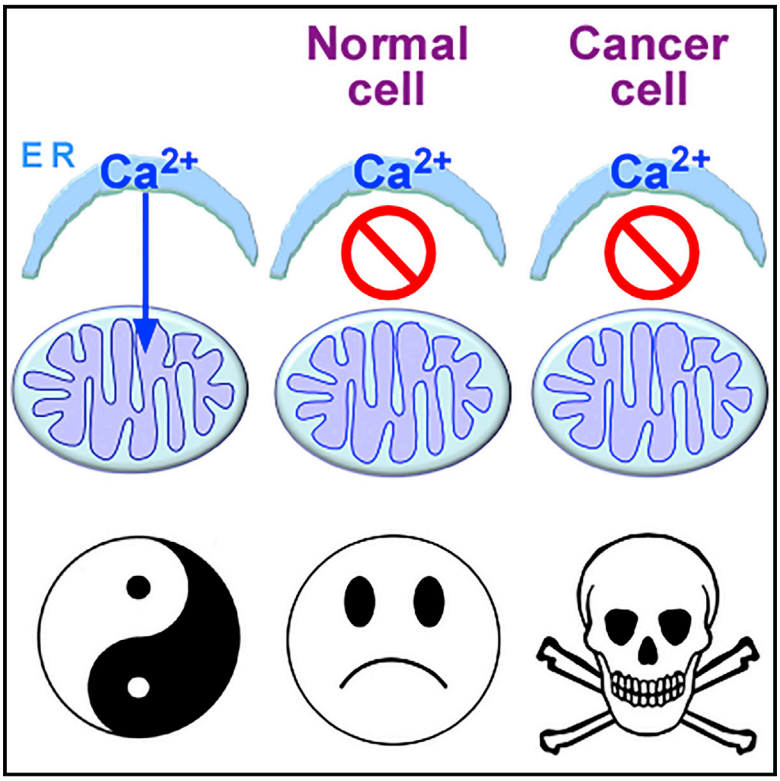

Authors

César Cárdenas, Marioly Müller, Andrew McNeal, ..., J. Alan Diehl, Todd W. Ridky, J. Kevin Foskett

Correspondence

jcesar@u.uchile.cl (C.C.), foskett@mail.med.upenn.edu (J.K.F.)

In Brief

Cárdenas et al. show that inhibition of low-level ER-to-mitochondria Ca^{2+} transfer is toxic, specifically to cancer cells. Their study reveals an unexpected dependency on constitutive Ca^{2+} transfer to mitochondria for viability of tumorigenic cells and suggest that mitochondrial Ca^{2+} addiction is a novel feature of cancer cells.

Highlights

- Low-level ER-to-mitochondria Ca^{2+} flux maintains ATP levels in cells
- Absence of basal mitochondrial Ca^{2+} uptake induces autophagy
- Autophagy protects normal cells but is insufficient for survival of cancer cells
- Cancer cells fundamentally require basal mitochondrial Ca^{2+} uptake for survival

Cárdenas et al., 2016, Cell Reports *14*, 2313–2324
March 15, 2016
http://dx.doi.org/10.1016/j.celrep.2016.02.030

CellPress

Cell Reports
Article

Selective Vulnerability of Cancer Cells by Inhibition of Ca^{2+} Transfer from Endoplasmic Reticulum to Mitochondria

César Cárdenas,[1,*] Marioly Müller,[2] Andrew McNeal,[3] Alenka Lovy,[4] Fabian Jaňa,[1] Galdo Bustos,[1] Felix Urra,[1] Natalia Smith,[1] Jordi Molgó,[5] J. Alan Diehl,[6,9] Todd W. Ridky,[3] and J. Kevin Foskett[7,8,*]
[1]Anatomy and Developmental Biology Program, Institute of Biomedical Sciences, Geroscience Center for Brain Health and Metabolism, University of Chile, Santiago, Chile
[2]Department of Medical Technology, Faculty of Medicine, University of Chile, Santiago, Chile
[3]Department of Dermatology, Perelman School of Medicine, University of Pennsylvania, Philadelphia, PA 19104, USA
[4]Center for Neuroscience Research, Tufts University School of Medicine, Boston, MA 02111, USA
[5]CEA, iBiTecS, Service d'Ingénierie Moléculaire des Protéines, Laboratoire de Toxinologie Moléculaire et Biotechnologies, Bâtiment 152, Courrier Number 24, 91191 Gif-sur-Yvette, France
[6]Department of Cancer Biology, Perelman School of Medicine, University of Pennsylvania, Philadelphia, PA 19104, USA
[7]Department of Physiology, Perelman School of Medicine, University of Pennsylvania, Philadelphia, PA 19104, USA
[8]Department of Cell and Developmental Biology, Perelman School of Medicine, University of Pennsylvania, Philadelphia, PA 19104, USA
[9]Present address: Department of Biochemistry and Molecular Biology, Medical University of South Carolina, Charleston, SC 29403, USA
*Correspondence: jcesar@u.uchile.cl (C.C.), foskett@mail.med.upenn.edu (J.K.F.)
http://dx.doi.org/10.1016/j.celrep.2016.02.030

SUMMARY

In the absence of low-level ER-to-mitochondrial Ca^{2+} transfer, ATP levels fall, and AMPK-dependent, mTOR-independent autophagy is induced as an essential survival mechanism in many cell types. Here, we demonstrate that tumorigenic cancer cell lines, transformed primary human fibroblasts, and tumors in vivo respond similarly but that autophagy is insufficient for survival, and cancer cells die while their normal counterparts are spared. Cancer cell death is due to compromised bioenergetics that can be rescued with metabolic substrates or nucleotides and caused by necrosis associated with mitotic catastrophe during their proliferation. Our findings reveal an unexpected dependency on constitutive Ca^{2+} transfer to mitochondria for viability of tumorigenic cells and suggest that mitochondrial Ca^{2+} addiction is a feature of cancer cells.

INTRODUCTION

Inositol 1,4,5-trisphosphate receptors ($InsP_3Rs$) are a ubiquitous family of Ca^{2+} release channels present primarily in the ER (Foskett et al., 2007). Ca^{2+} release through the $InsP_3R$ regulates numerous cell functions, including transcription, proliferation, secretion, and motility, among others (Cárdenas et al., 2005; Foskett et al., 2007). $InsP_3R$-mediated Ca^{2+} signals also regulate cell metabolism, primarily by supplying released Ca^{2+} to mitochondria, where it stimulates production of reducing equivalents by pyruvate dehydrogenase (PDH) and two Ca^{2+} dependent dehydrogenases in the tricarboxylic acid (TCA) cycle, α-ketoglutarate dehydrogenase (α-KGDH) and isocitrate dehydrogenase (IDH) (McCormack and Denton, 1979), as well as activities of respiratory chain components to promote oxidative phosphorylation (OXPHOS) and ATP production (Murphy et al., 1990; Territo et al., 2000). Low-level constitutive $InsP_3R$-mediated Ca^{2+} release is essential for maintaining basal levels of OXPHOS and ATP production in a wide variety of cell types (Cárdenas et al., 2010). In the absence of constitutive ER-to-mitochondrial Ca^{2+}-transfer, ATP levels fall and AMPK-dependent, mTOR (mammalian target of rapamycin)-independent autophagy is induced (Cárdenas et al., 2010; Mallilankaraman et al., 2012a, 2012b) as an essential survival mechanism (Cárdenas et al., 2010). In all cell types examined, inhibition of constitutive mitochondrial Ca^{2+} uptake induced a bioenergetic crisis that resulted in a reprogramming of metabolism reminiscent of that induced by nutrient starvation, despite nutrient availability and enhanced nutrient uptake.

A hallmark feature of cancer cells is a re-programming of their metabolism, even when nutrients are available (Boroughs and DeBerardinis, 2015; Jones and Thompson, 2009; Jose et al., 2011). All major tumor suppressors and oncogenes have connections with metabolic pathways (Deberardinis et al., 2008; Koppenol et al., 2011; Levine and Puzio-Kuter, 2010; Vander Heiden et al., 2009). Warburg suggested that cancer originates from irreversible injury in mitochondria, followed by a compensatory increase of glycolysis (Warburg, 1956), but increasing evidence indicates that mitochondrial function is essential for cancer cells (Koppenol et al., 2011). A continuous supply of metabolic intermediates from the TCA cycle fuels lipid, nucleic acid, and protein biosynthesis and provides redox power essential for cancer cell proliferation (Boroughs and DeBerardinis, 2015; Deberardinis et al., 2008). Many tumor cells require

OXPHOS to maintain growth (Birsoy et al., 2014; Caro et al., 2012) and for the majority of their ATP production (Jose et al., 2011). Mutations in OXPHOS genes are tumorigenic (Bayley and Devilee, 2010), and mitochondrial inhibitors have antitumor activity (Cheng et al., 2012; Momose et al., 2010; Zhang et al., 2014).

Accordingly, here, we asked what role constitutive mitochondrial Ca^{2+} uptake, important in normal cell bioenergetics, plays in cancer cell metabolism and viability. Using tumorigenic breast and prostate cancer cell lines and genetically transformed isogenic primary human fibroblasts, we found that interruption of constitutive ER-to-mitochondrial Ca^{2+} transfer elicited effects similar to those observed in normal cells, including diminished OXPHOS, AMPK activation, and induction of autophagy. Whereas autophagy was sufficient for survival of normal cells, it was insufficient in cancer cells, which responded strikingly with massive death, while their normal counterparts were spared. Furthermore, inhibition of $InsP_3R$ activity strongly suppressed melanoma tumor growth in mice. Addition of metabolic substrates or nucleotides rescued the lethal effect of inhibiting mitochondrial Ca^{2+} uptake, suggesting that cell death was induced by compromised bioenergetics. Cell death was caused by necrosis associated with mitotic catastrophe at daughter cell separation during ongoing proliferation of the cancer cells. Our findings reveal a fundamental and unexpected dependency on $InsP_3R$-mediated Ca^{2+} transfer to mitochondria for viability of cancer cells.

RESULTS

Inhibition of $InsP_3R$ Activity Creates a Bioenergetic Crisis in Both Tumorigenic and Non-tumorigenic Cell Lines

We examined the effects of $InsP_3R$ inhibition on metabolic responses of human breast- and prostate-cancer-derived tumorigenic cell lines. As controls, we examined non-tumorigenic lines derived from normal tissues. XeB (5 μM, 1 hr), a specific $InsP_3R$ inhibitor (Jaimovich et al., 2005), reduced basal and maximal oxygen consumption rates (OCRs) (Figure 1A), enhanced AMPK phosphorylation (P-AMPK) (Figure 1B), and induced autophagic flux in both non-tumorigenic and tumorigenic breast (Figures 1C, S1A, and S1B) and prostate (Figures S2A and S2B) cell lines. The effects of XeB on bioenergetic parameters were dose dependent, with 5 μM as the minimum concentration required to strongly induce autophagy and significantly reduce basal and maximal OCRs in both MCF10A and MCF7 cells (Figures S1C–S1F). Similar responses to $InsP_3R$ inhibition, including decreased OCR, increased P-AMPK, and induction of autophagy were observed in mouse melanoma B16F10 cells (Figures S2F–S2H), demonstrating that this is a non-species-specific general phenomenon. Thus, XeB generates similar bioenergetic crises in tumorigenic and non-tumorigenic cell lines. XeB inhibited constitutive and spontaneous Ca^{2+} transients in both MCF10A and MCF7 cells (Figures 1D and S1G; Movie S1 [MCF7]; Movie S2 [MCF10A]). Furthermore, simultaneous genetic knockdown (KD) of $InsP_3R$ types 1 and 3 (~50%–70% efficiency; Figure S1H), the main isoforms expressed in these cells (Figures S1I–S1K), created a similar bioenergetic crisis in normal and tumorigenic cells (Figures 1E and 1F).

Inhibition of $InsP_3R$ Activity Is Toxic, Specifically for Tumorigenic Cells

Breast cells were treated with XeB for 24 hr, and cell viability was assessed by flow cytometry. 2.5 μM XeB had little effect, except for tumorigenic HS578T cells, in which death was enhanced by 8% ± 1% (Figure 2A). In contrast, 5 μM XeB induced substantial death by 43% ± 4% and 53% ± 2% in tumorigenic MCF7 and T47D cell lines, respectively, and over 22% ± 1% in HS578T cells. In contrast, non-tumorigenic MCF10A cells showed only limited sensitivity (5% ± 0.4% cell death). At 10 μM, XeB killed 63% ± 7% and 64% ± 5% of MCF7 and T47D cells, respectively, and 42% ± 6% of HS578T cells, whereas MCF10A cells had only modest sensitivity (24% ± 1%) (Figure 2A). Similar XeB-mediated killing was observed in human-cancer-derived prostate cell lines PC3 and DU145, but there was little effect for the non-tumorigenic PNT2 prostate line (Figure S2C). In agreement with results from flow cytometry, XeB caused striking lactate dehydrogenase (LDH) release in all tumorigenic breast lines, compared with MCF10A cells (Figure 2B), as well as in mouse melanoma B16F10 cells (Figure S2I). As assessed by both flow cytometry and LDH release (Figures 2C and 2D), tumorigenic lines started dying as early as at 6 hr of exposure to 5 μM XeB, while the non-tumorigenic cells remained insensitive. The observed differences in XeB sensitivity could not be accounted for by intrinsic differences in proliferation rates between cell lines in untreated conditions (Figures S1L and S2E). Tumorigenic breast (Figure 2E) and prostate (Figure S1D) cells exposed to XeB (5 μM for 24 hr) displayed striking morphological changes, including rounding up and shrinkage, whereas similarly treated non-tumorigenic cells maintained normal morphology.

These results suggest that tumor cell survival is dependent upon $InsP_3R$ signaling. In agreement, inhibition of phospholipase C (PLC), the enzyme responsible for the generation of the $InsP_3R$ ligand $InsP_3$, with U73122 (2 μM), but not the inactive analog U73343, caused striking LDH release in all tumorigenic breast cell lines, with substantially less effects in the non-tumorigenic line (Figure 2F). Similarly, simultaneous genetic KD of $InsP_3R$ types 1 and 3 caused comparable LDH release as XeB and U73122 in MCF7 and T47D cells, while non-tumorigenic MCF10A cells showed only a small increase (Figure 2G). Thus, tumorigenic cell lines appear to have an essential dependence on $InsP_3R$-mediated Ca^{2+} signaling for survival, unlike normal cells.

Inhibition of $InsP_3R$ Activity Reduces the Proliferative Potential of Cancer Cell Lines

Colony formation is a hallmark of cancer cells that reflects their ability to proliferate indefinitely (Munshi et al., 2005). XeB (5 μM, 24 hr) diminished colony formation by tumorigenic breast MCF7 (Figure 3A) and T47D cells and prostate PC3 cells (Figures S3A and S3B). In normal cells, the bioenergetic crisis caused by inhibition of $InsP_3R$ activity could be overcome by providing pyruvate as a mitochondrial substrate, presumably by mass action to drive flux through the system (Cárdenas et al., 2010). Methyl-pyruvate (5 μM, 24 hr) rescued the XeB-induced MCF7 colony formation defect (Figure 3B). Pyruvate has antioxidant properties (Andrae et al., 1985). However, XeB did not enhance reactive oxygen species (ROS) production (Figure S3C), and

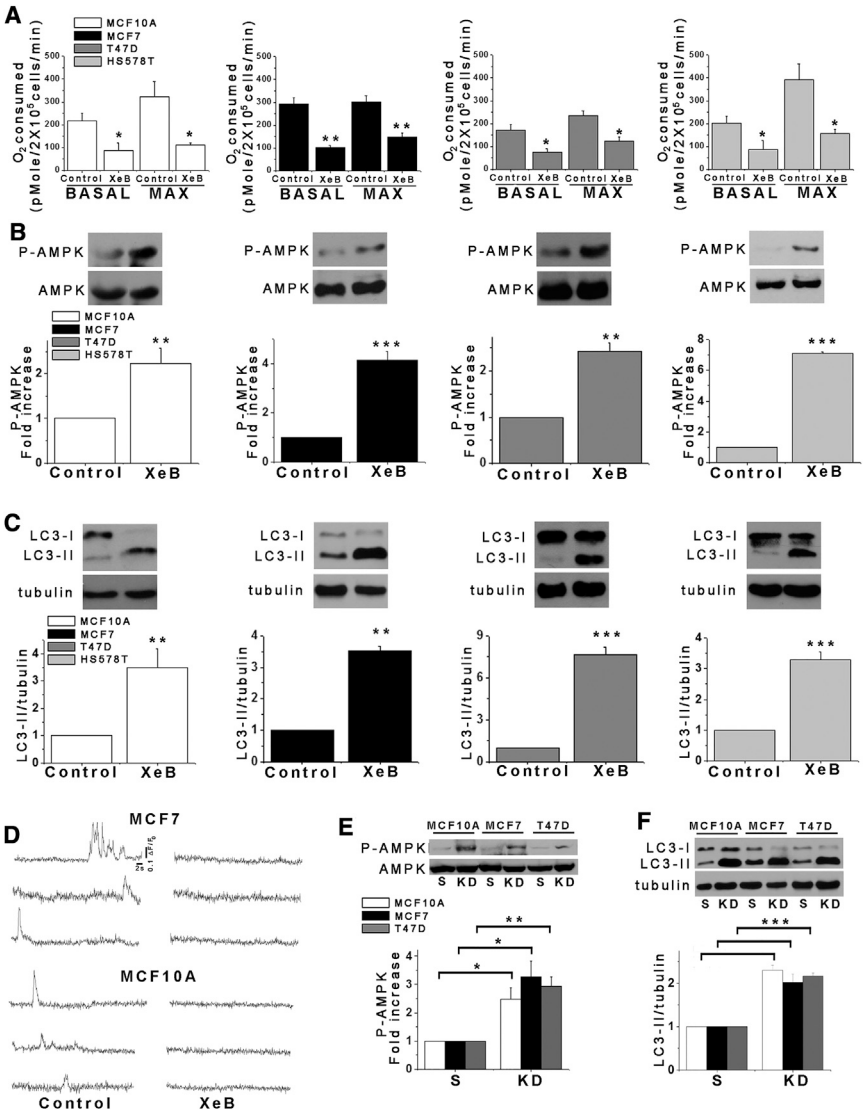

Figure 1. Inhibition of $InsP_3R$ Activity Reduces Oxygen Consumption and Activates AMPK-Dependent Autophagy

(A) Basal and maximal OCRs of non-tumorigenic and tumorigenic breast cell lines incubated with 5 μM XeB for 1 hr. n = 3, mean ± SEM. *p < 0.05; **p < 0.01 (Student's t test).

(B) Representative western blots of P-AMPK and total AMPK in non-tumorigenic and tumorigenic breast cell lines incubated with 5 μM XeB for 1 hr. Bar graph: P-AMPK/AMPK expressed as average fold increase over basal levels (control cells). n = 5, mean ± SEM. **p < 0.01; ***p < 0.001 (Student's t test).

(C) Representative western blots of autophagy marker LC3 or tubulin as loading control in non-tumorigenic and tumorigenic breast cell lines treated with 5 μM XeB (1 hr) and quantification of LC3-II/tubulin expressed as fold increase over basal levels (control cells). n = 5, mean ± SEM. **p < 0.01; ***p < 0.001 (Student's t test).

(D) Representative fluorescence recordings of Ca^{2+} release events in unstimulated MCF7 and MCF10A cells treated (or not treated) with 5 μM XeB (see also Movies S1 and S2).

(E) Representative western blots of AMPK in breast lines transiently transfected with a small interfering RNA (siRNA) against both type 1 and type 3 $InsP_3R$ (KD) or non-target scrambled (S) siRNA for 24 hr. Bar graph: P-AMPK/AMPK expressed as average fold increase over basal levels (S cells). n = 3, mean ± SEM. *p < 0.05; **p < 0.01 (Student's t test).

(F) Representative western blots of LC3 or tubulin in breast cells transiently transfected with a siRNA against type 1 and type 3 $InsP_3R$ (KD) or a non-target (S) siRNA for 24 hr and quantification of LC3-II/tubulin expressed as average fold increase over basal levels (S cells). n = 3, mean ± SEM. ***p < 0.001 (Student's t test).

See also Figure S1 and Movies S1 and S2.

N-acetylcysteine (NAC) (5 mM, 24 hr) did not rescue colony formation (Figure 3B) or prevent XeB-induced AMPK activation (Figure S3D), autophagy (Figure S3E), or MCF7 cell death (Figure S3F). These results suggest that cancer cell killing and reduction of colony formation by inhibition of $InsP_3R$ activity is a consequence of a bioenergetic crisis that can be rescued by a mitochondrial substrate, but not by an antioxidant.

XeB Induces Cell Death in Transformed, But Not Isogenic Control, Human Fibroblasts

Although the cell lines are well validated and broadly used models, the fact that the control lines are also transformed complicates the results. Therefore, we turned to an isogenic primary human fibroblast model. Primary human fibroblasts were transformed by the incorporation of oncogenic $HRas^{G12V}$ while bypassing retinoblastoma (Rb)-mediated G1 cell-cycle restraint by enforced expression of cyclin-dependent kinase-4 (Cdk4) (Ridky et al., 2010). This model (HrasG12V-CDK4) has classic cancer features, including invasive properties. HrasG12V-CDK4 fibroblasts showed elevated glucose consumption (Figure S3G) and lactate release (Figure S3H), consistent with acquisition of a Warburg-type metabolism. Nevertheless, control and transformed cells had comparable OCRs, suggesting similar OXPHOS (Figure 4A). Furthermore, the OCR was reduced by XeB to a similar extent in HrasG12V-CDK4 and isogenic control cells (Figure 4A), and a bioenergetic crisis ensued, as evidenced by increased P-AMPK and induction of autophagy (Figures 4B and 4C). These results suggest that mitochondria remain important for maintenance of cell bioenergetics in these primary transformed cells.

As in the cancer cell lines, XeB induced profound morphological changes and reduced the number of HrasG12V-CDK4 cells per field, whereas isogenic controls behaved similarly to vehicle-treated cells (Figure S3I). LDH release was enhanced 6-fold in HrasG12V-CDK4 cells, compared with isogenic controls (Figure 4D). The sensitivity of HrasG12V-CDK4 cells compared with

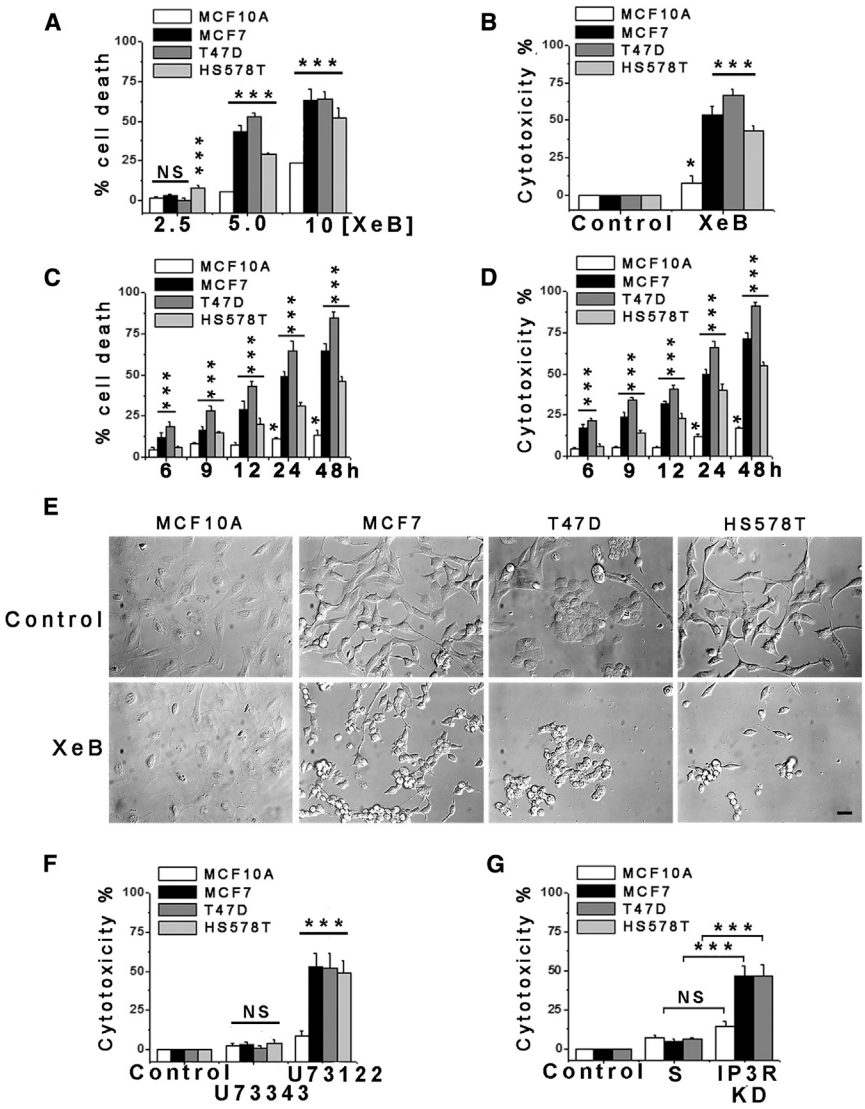

Figure 2. Inhibition of $InsP_3R$ Causes Death of Tumorigenic Breast Cell Lines

(A) Non-tumorigenic and tumorigenic human breast cell lines were treated with XeB for 24 hr, and cell death was determined by TOTO-3 incorporation by flow cytometry. n = 3, mean ± SEM. ***p < 0.001; NS, not significant (one-way ANOVA followed by Dunnett's multiple comparison post test).

(B) Breast cell lines were treated with 5 μM XeB for 24 hr, and cell death was determined by LDH release. n = 3, mean ± SEM. *p < 0.05; ***p < 0.001 (Student's t test).

(C) Time course of cell death determined by TOTO-3 incorporation by flow cytometry in human breast cell lines treated with 5 μM XeB. n = 3, mean ± SEM. *p < 0.05; ***p < 0.001 (Student's t test).

(D) Time course of cell death determined by LDH release in breast cell lines treated with 5 μM XeB. n = 3, mean ± SEM. *p < 0.05; ***p < 0.001 (Student's t test).

(E) Differential interference contrast (DIC) images of breast cell lines derived from non-tumorigenic (MCF10A) or tumorigenic (MCF7, T47D, HS578T) human tissue treated with 5 μM XeB for 24 hr. Scale bar represents 10 μm. n = 3.

(F) Non-tumorigenic and tumorigenic breast cell lines were treated with 2 μM of the PLC inhibitor U73122 or its inactive analog U73343 for 12 hr, and cell death was determined by LDH release. n = 3, mean ± SEM. ***p < 0.001; NS, not significant (Student's t test).

(G) Cell death (LDH release) in human breast cell lines transiently transfected with a siRNA against type 1 and type 3 $InsP_3R$ (IP3R KD) or a scrambled non-target (S) siRNA for 24 hr. n = 3, mean ± SEM. ***p < 0.001; NS, not significant (Student's t test). See also Figure S1.

that of isogenic cells could not be accounted for by differences in their normal rates of proliferation (Figure S3J). Simultaneous KD of $InsP_3R$ types 1 and 3, the main isoforms in these cells (Figures S4A–S4D) enhanced P-AMPK and autophagy in both HrasG12V-CDK4 and isogenic control fibroblasts (Figure 4E and 4F), but it caused significant death, specifically in the HrasG12V-CDK4 cells (Figure 4G). Thus, in primary human cells, as in breast and prostate cell lines, inhibition of $InsP_3R$ activity is strongly toxic specifically for cancer cells.

Killing of Cancer Cells by Inhibition of $InsP_3R$ Activity Is Mediated by Altered Mitochondrial Function

In normal cells, inhibition of mitochondrial Ca^{2+} uptake phenocopies the effects of $InsP_3R$ inhibition on cell bioenergetics, suggesting that the primary role of $InsP_3R$ activity in preserving normal cellular bioenergetics is to provide Ca^{2+} to mitochondria (Mallilankaraman et al., 2012a). The similar bioenergetic responses to inhibition of $InsP_3R$ activity of tumor cell lines and HrasG12V-CDK4 cells suggested that cancer cells may have a similar dependence on constitutive mitochondrial Ca^{2+} uptake. To test this, we knocked down in HrasG12V-CDK4 and isogenic control cells the expression of MCU, the pore-forming subunit of the mitochondrial uniporter Ca^{2+} channel, the major Ca^{2+} uptake pathway in mitochondria (Foskett and Philipson, 2015). MCU expression was similar in human normal versus transformed fibroblasts or between the MCF10A and MCF7 cells (Figures S4E and S4F). MCU KD (Figure S4E) increased P-AMPK and induced autophagy (Figures 4E and 4F), as in normal cells (Mallilankaraman et al., 2012a, 2012b). Importantly, MCU KD enhanced killing preferentially of the HrasG12V-CDK4-transformed cells (Figure 4G). In contrast, overexpression of MCU was unable to protect MCF7 cells from death induced by $InsP_3R$ inhibition with XeB (Figures S4G and S4H). These results suggest that $InsP_3R$-mediated Ca^{2+} release and its transfer to mitochondria through MCU are essential to maintain cancer cell viability.

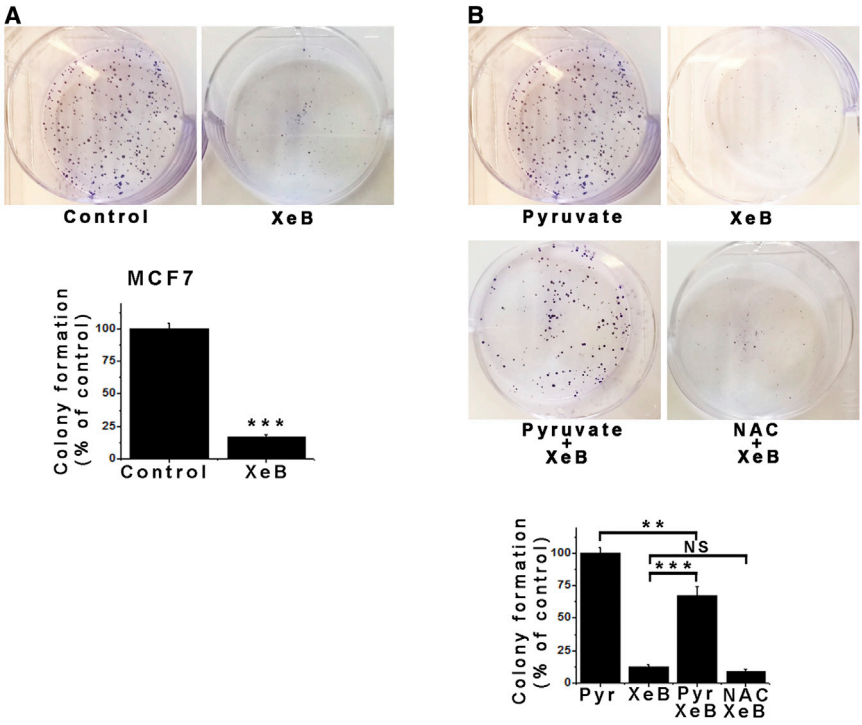

Figure 3. Inhibition of $InsP_3R$ Signaling Impairs Colony Formation in the MCF7 Tumorigenic Breast Cell Line

(A) Representative plates of MCF7 cells treated with 5 μM XeB or vehicle (top) and quantitative analysis of colony numbers (bottom). n = 3, mean ± SEM. ***p < 0.001 (Student's t test).

(B) Representative plates of MCF7 cells treated with 5 μM XeB, 5 mM methyl-pyruvate, 5 μM XeB + 5 mM methyl-pyruvate, or 5 μM XeB + 5 mM n-acetylcysteine (NAC) (top) and quantitative analysis of colony numbers (bottom). n = 3, mean ± SEM. **p < 0.001; ***p < 0.001; NS, not significant (Student's t test).

See also Figure S2.

The TCA cycle is regulated by product inhibition, substrate availability, and cofactors, including Ca^{2+}. PDH, IDH, and α-KGDH activities are all critically regulated by mitochondrial matrix Ca^{2+} (Glancy and Balaban, 2012). Inhibition of $InsP_3R$-mediated Ca^{2+} release reduces PDH activity, resulting in decreased OCR and ATP production (Cárdenas et al., 2010). Cancer cells rely on mitochondria for production of TCA intermediates needed for high growth and proliferation (Boroughs and DeBerardinis, 2015). We speculated that inhibition of mitochondrial function by the absence of sufficient matrix Ca^{2+} cannot be compensated for, specifically in cancer cells, because of this dependence on the TCA cycle. Addition of dimethyl α-KG or methyl-pyruvate, two substrates that energize mitochondria (Cárdenas et al., 2010; Wise and Thompson, 2010) to XeB-treated (5 μM, 24 hr) fibroblasts strongly reduced cell death (Figure 4H). Protection was unrelated to antioxidant properties of the substrates, since NAC (5 mM) was without effect on XeB-induced P-AMPK (Figures S4I and 4K), autophagy (Figures S4J and S4L), or killing (Figure S4M).

Although enhanced P-AMPK indicates that inhibition of $InsP_3R$-mediated Ca^{2+} transfer to mitochondria lowers cellular ATP (Cárdenas et al., 2010), glycolysis is believed to provide sufficient ATP for cancer cell functions (Deberardinis et al., 2008). However, as highly proliferative cells, cancer cells rely on the TCA cycle for the production of metabolic intermediates for the generation of fatty acids and nucleotides. At least three mitochondrial pathways are involved in pyrimidine and purine nucleotide synthesis, and the rate-limiting step in de novo synthesis of pyrimidines occurs in mitochondria and is linked to respiratory chain activity (Desler et al., 2010). To determine whether mitochondrial hypo-function in response to $InsP_3R$ inhibition compromises nucleotide metabolism that may contribute to cancer cell death, HrasG12V-CDK4 fibroblasts were treated with 5 μM XeB for 24 hr in media supplemented with nucleosides. Notably, nucleoside supplementation was strongly protective of XeB-treated HrasG12V-CDK4 cells (Figure 5A), despite enhanced P-AMPK phosphorylation and autophagy activation (Figures 5B–5E). Thus, with nucleoside supplementation, cancer cells behave as normal cells, surviving in the face of an unfavorable bioenergetic state.

Nucleosides contribute to the purine and pyrimidine generation necessary for DNA synthesis. In normal fibroblasts, XeB (5 μM, 10 hr) reduced bromodeoxyuridine (BrdU) incorporation by >50% (Figure 5F), suggesting that the unfavorable bioenergetic state in the absence of Ca^{2+} transfer to mitochondria slowed cell proliferation, as expected. In marked contrast, XeB had minimal effects on BrdU incorporation into HrasG12V-CDK4 cells (Figure 5G). These results suggest that normal cells restrain entry into the S phase when conditions are unsuitable, but transformed cells do not recognize this checkpoint. Because of the enforced expression of Cdk4 in HrasG12V-CDK4 cells, it remained unclear whether other cancer cells would progress similarly into mitosis during a XeB-induced compromised bioenergetic state. XeB (5 μM, 24 hr) increased the population of MCF10A cells in the G1 phase that correlated with a decrease proceeding through the S phase (Figure 5H), as observed in normal human primary fibroblasts. In contrast, MCF7 cells showed no increase of the G1 population and only a slight decrease in cells in the S phase (Figure 5I). This suggests that MCF7 cells, like HrasG12V-CDK4 cells but unlike normal cells, proceed through the cell cycle, despite their compromised bioenergetic state. Similar behavior was observed in HeLa cells, a common cervical tumor cell line (Figure 5J).

HeLa cells were optically imaged to observe progression through the cell cycle. Remarkably, XeB-treated cells entered mitosis but then collapsed catastrophically and died during daughter cell separation (n = 30 mitoses) (Figure 5L; Movie S3), a phenotype never observed in vehicle-treated cells (n = 50 mitoses). This suggests that, in cells with $InsP_3R$ activity inhibited

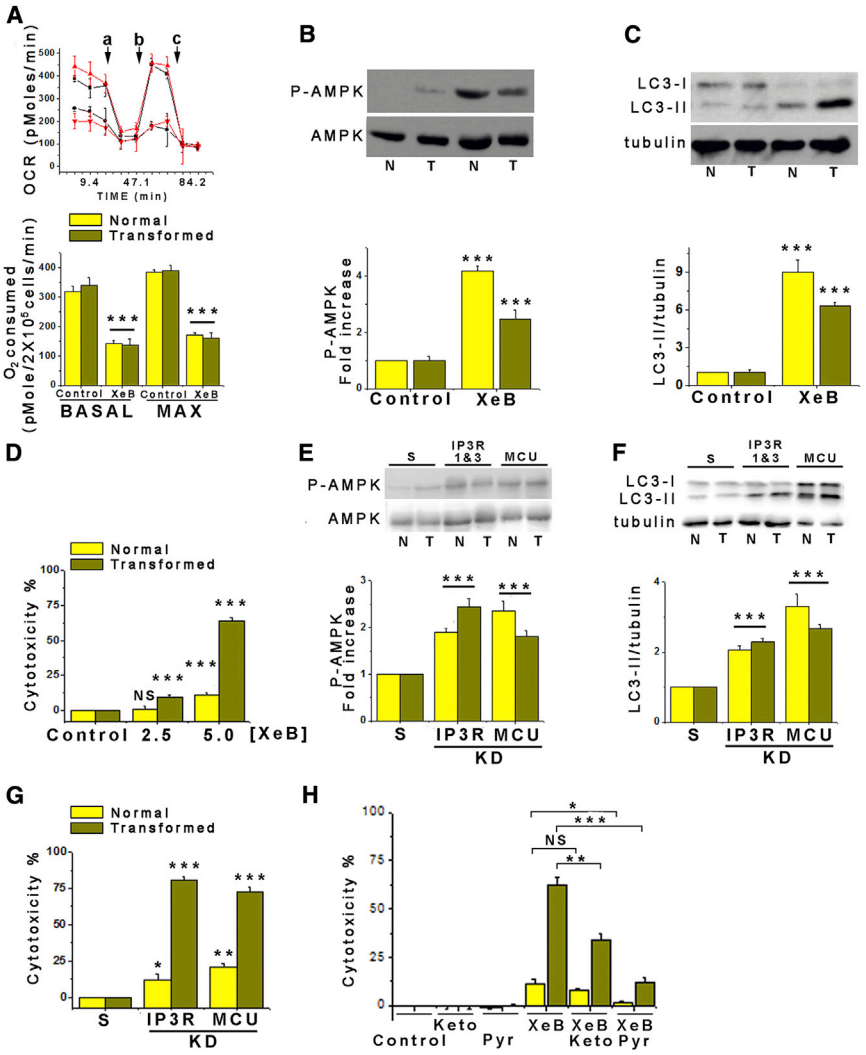

Figure 4. Pharmacological and Genetic Inhibition of $InsP_3R$ Causes Death of Primary HRasG12V-Cdk4 Transformed Human Fibroblasts

(A) Top: representative traces of OCR in normal (black) or transformed (red) fibroblasts treated (black circles, red upside-down triangles) or not (black squares, red triangles) with 5 μM XeB for 1 hr. a: injection of 1 μM oligomycin; b: 300 nM FCCP; c: 100 nM rotenone. Bottom: summary of basal and maximal OCRs in fibroblasts treated, or not treated, with 5 μM XeB for 1 hr. n = 3, mean ± SEM. ***p < 0.001.

(B) Representative western blots of AMPK in normal (N) and transformed (T) fibroblasts treated with 5 μM XeB (1 hr). Bar graph: P-AMPK/AMPK expressed as average fold increase over basal levels (control cells). n = 6, mean ± SEM. ***p < 0.001 (Student's t test).

(C) Representative western blots of LC3 and tubulin in normal (N) and transformed (T) fibroblasts treated with 5 μM XeB for 1 hr. Bar graph: LC3-II/tubulin expressed as average fold increase over basal levels (control cells). n = 6, mean ± SEM. ***p < 0.001 (Student's t test).

(D) Determination of cell death by LDH release in normal and transformed fibroblasts treated with 2.5 or 5 μM XeB (24 hr). n = 3, mean ± SEM. ***p < 0.001; NS, not significant (Student's t test).

(E) Representative western blots of AMPK in normal (N) and transformed (T) fibroblasts transiently transfected with a siRNA against type 1 and type 3 $InsP_3R$ (IP3R) for 24 hr or siRNA against MCU for 72 hr. Bar graph: P-AMPK/AMPK expressed as the average fold increase over basal levels (S cells). n = 3, mean ± SEM. ***p < 0.001 (Student's t test).

(F) Representative western blots of LC3 and tubulin in normal (N) and transformed (T) fibroblasts transiently transfected with a siRNA against type 1 and type 3 $InsP_3R$ for 24 hr or siRNA against MCU for 72 hr, or scrambled sRNAs (S); LC3-II/tubulin expressed as average fold increase over basal levels (S cells). n = 3, mean ± SEM. ***p < 0.001 (Student's t test).

(G) Determination of cell death by LDH release in normal and transformed fibroblasts transiently transfected with a siRNA against type 1 and type 3 $InsP_3R$ for 24 hr or siRNA against MCU for 72 hr. n = 3, mean ± SEM. *p < 0.05; **p < 0.01; ***p < 0.001 (Student's t test).

(H) Determination of cell death by LDH release in normal and transformed fibroblasts treated simultaneously with 5 μM XeB and either 5 mM methyl-pyruvate (Pyr) or 5 mM dimethyl α-KG (Keto) for 24 hr. n = 3, mean ± SEM. *p < 0.05; **p < 0.01; ***p < 0.001; NS, not significant (Student's t test).

See also Figure S4.

or mitochondrial Ca^{2+} uptake otherwise blocked, cancer cells progress through the cell cycle, despite their bioenergetic crisis, in contrast to normal cells that stop in the G1 phase, and their progression into mitosis appears to be a step that results in cell death. To probe this further, MCF7 cells were incubated with 400 μM hydroxyurea (HU) to arrest them in the S phase of the cell cycle (Figure S5A) and then were treated with 5 μM XeB for 24 hr. As shown in Figure 5K, the prevention of cell-cycle progression strongly decreased cell death induced by XeB.

Cell Death Induced by Inhibition of $InsP_3R$ Ca^{2+} Signaling Is Mainly Necrotic

Our results reveal that inhibition of $InsP_3R$-mediated Ca^{2+} transfer to mitochondria causes death, specifically in tumorigenic cells, but how they die is unknown. Autophagy inhibition with 3-methyladenine (3MA) (Figures S5B and S5C) did not prevent cell death in XeB-treated MCF7 and MCF10A cells (Figure 6A) and in normal and HrasG12V-CDK4 fibroblasts (Figure 6B), suggesting that autophagy is not driving cell death. Although 3MA tended to increase cell death in XeB-treated MCF10A cells and normal fibroblasts, suggesting that autophagy plays a cell survival role, as previously suggested (Cárdenas et al., 2010), KD of ATG7 (Figures S5D and S5E) did not influence the extent of cell death (Figure S5F). Inhibition of apoptosis with the pan-caspase inhibitor Z-VAD-FMK did not protect tumorigenic cells from XeB-induced death (Figures 6A and 6B). Furthermore, western blot and immunofluorescence analyses of activated cleaved caspase-3 in human normal and HrasG12V-CDK4 fibroblasts

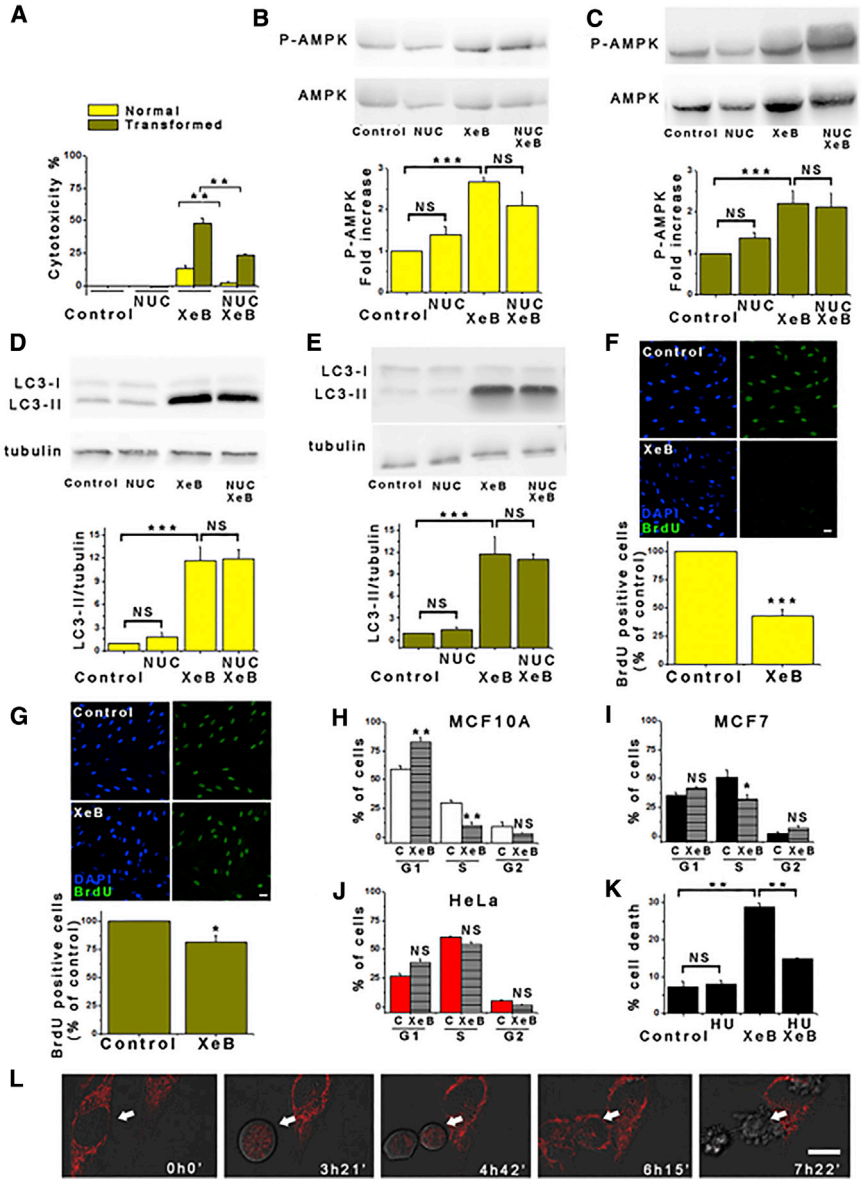

Figure 5. Nucleoside Rescue of Cancer Cell Killing and Cell Cycle Defects by Inhibition of $InsP_3R$ Activity

(A) Normal and transformed fibroblasts were treated with 5 μM XeB in the absence or presence of nucleosides (NUC) for 24 hr, and cell death was determined by LDH release. n = 3, mean ± SEM. **p < 0.01 (Student's t test).

(B) Representative western blots of AMPK in normal fibroblasts treated with 5 μM XeB for 1 hr in the presence or absence of nucleosides (NUC). Bar graph: P-AMPK/AMPK expressed as average fold increase over basal levels (control cells). n = 3, mean ± SEM. ***p < 0.001; NS, not significant (Student's t test).

(C) Same as in (B), using transformed fibroblasts. n = 3, mean ± SEM. ***p < 0.001; NS, not significant (Student's t test).

(D) Representative western blots of LC3 and tubulin in normal fibroblasts treated with 5 μM XeB for 1 hr in the presence or absence of nucleosides (NUC). Bar graph: LC3-II/tubulin expressed as average fold increase over basal levels (control cells). n = 3; mean ± SEM. ***p < 0.001; NS, not significant (Student's t test).

(E) Same as in (D), using transformed fibroblasts. n = 3, mean ± SEM. ***p < 0.001 (Student's t test).

(F) BrdU incorporation in normal fibroblasts treated with 5 μM XeB for 12 hr. Top: BrdU immunofluorescence. Bottom: BrdU labeling expressed as percentage of control. n = 3, mean ± SEM. ***p < 0.001 (Student's t test). Scale bar represents 10 μm.

(G) Same as in (F), using transformed fibroblasts. n = 3, mean ± SEM. *p < 0.05 (Student's t test). Scale bar represents 10 μm.

(H) Cell-cycle profile determined by flow cytometry in MCF10A cells treated, or not treated, with 5 μM XeB for 24 hr, showing percentage of cells in each phase. n = 3, mean ± SEM. **p < 0.001; NS, not significant.

(I) Cell-cycle profile in MCF7 cells treated, or not treated, with 5 μM XeB for 24 hr, showing the percentage of cells in each phase. n = 3, mean ± SEM. *p < 0.05, NS: not significant.

(J) As in (I), using HeLa cells. n = 3, mean ± SEM. NS: not significant.

(K) Cell death was determined by PI incorporation by flow cytometry of MCF7 cells treated, or not treated, with 5 μM XeB for 24 hr after a 48-hr treatment with 400 μM HU. n = 3, mean ± SEM. **p < 0.001; NS, not significant (Student's t test).

(L) DIC images of HeLa cells loaded with 8 nM TMRE. XeB (5 μM) was added at time 0h0'; images were collected at indicated times. Arrow shows dividing cell. Scale bar represents 10 μm.

See also Movie S3.

(Figure S5G), and in tumor samples (Figure S5H), similarly suggested that apoptosis is not a major feature associated with cell killing. Flow cytometry analyses using fluorescein isothiocyanate (FITC)-Annexin V and propidium iodide (PI) labeling further confirmed the presence of only a small apoptotic cell population after XeB treatment (Figure S5I). Inhibition of necroptosis with necrostatin also did not prevent XeB-induced cell death (Figures 6A and 6B). The transcription factor HMGB1 is normally localized in the nucleus but is released into the cytoplasm during early stages of necrosis (Scaffidi et al., 2002). Most (>50%) MCF7 cells exposed to 5 μM XeB for 24 hr lost nuclear labeling, while untreated cells and treated MCF10A cells overwhelmingly maintained nuclear HMGB1 labeling (Figures 6C and 6D). Together with the imaging data, these results suggest that, in response to the inhibition of Ca^{2+} transfer to mitochondria, cancer cells die by necrosis, at approximately the time of daughter cell separation in mitosis.

Inhibition of $InsP_3R$ Activity Impairs Tumor Growth in Nude Mice

To evaluate whether $InsP_3R$ inhibition affected tumor growth in vivo, subcutaneous tumors were generated using B16F10

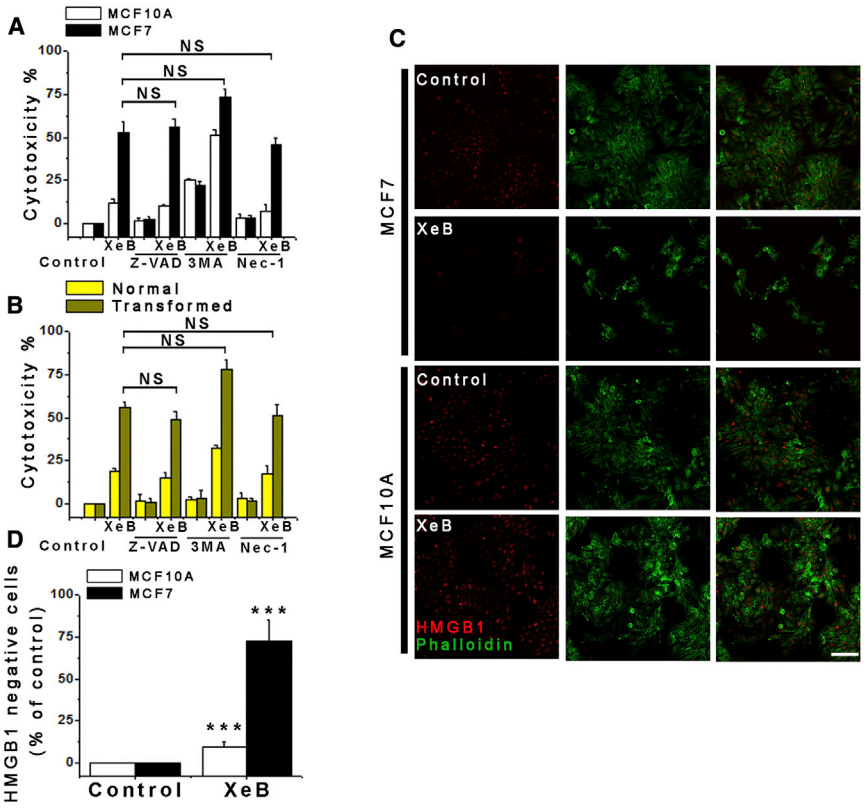

Figure 6. Inhibition of $InsP_3R$ Activity Kills Cancer Cells by Necrosis but Not by Autophagy, Apoptosis, or Necroptosis

(A) Non-tumorigenic (MCF10A) and tumorigenic (MCF7) breast cell lines were treated with 5 μM XeB for 24 hr in the presence or absence of the apoptosis inhibitor Z-VAD-FMK (20 μM), autophagy inhibitor 3-MA (10 mM), or necroptosis inhibitor nec-1 (20 μM), and cell death was determined by LDH release. n = 3, mean ± SEM. NS: not significant (Student's t test).

(B) Same as in (A) for normal and transformed primary human fibroblasts. n = 3, mean ± SEM. NS, not significant (Student's t test).

(C) HMGB1 immunofluorescence in MCF7 and MCF10A cells treated with 5 μM XeB or vehicle for 24 hr. Note that most nuclear label is absent in treated MCF7 cells. Scale bar represents 10 μm.

(D) Quantification of loss of nuclear HMGB1 expressed as percent increase over control. n = 3, mean ± SEM. ***p < 0.001 (Student's t test).

melanoma cells. As described earlier, treatment of B16F10 cells in vitro with 5 μM XeB induced AMPK phosphorylation and activated autophagy (Figures S2F and S2G). OCR was inhibited (Figure S2H), and LDH release was increased in a dose-dependent manner by a 24-hr exposure to XeB (Figure S2I). Thus, this cell line is appropriate to examine in vivo. B16F10 cells were injected subcutaneously into ventral flanks of 5- to 6-week-old nu/nu mice. When tumors were palpable, usually by day 5 post-injection, one tumoral flank was injected with 100 μl of a solution of 100 μM XeB, and the other was injected with vehicle (PBS plus ethanol). One day later, mice were euthanized, and tumors were extracted and weighed (Figure S6A, treatment 1). XeB reduced tumor size by nearly 60% in comparison to untreated tumors (Figure 7A). In a different paradigm, one tumoral flank was treated every other day for a week with 100 μl of a solution of 100 μM XeB (Figure S6A, treatment 2). XeB reduced tumor size by ~70%, compared with untreated tumors (Figure 7B). Markers of bioenergetic stress normally observed after $InsP_3R$ inhibition, including enhanced AMPK phosphorylation and autophagy, were observed in the XeB-injected tumor sections (Figures S6B and S6C). The vast majority of XeB-treated tumor cells lost HMGB1 nuclear localization, whereas control tumor cells had HMGB1 largely in the nucleus (Figure 7C). Ki67, a marker of cell proliferation, labeled nuclei equivalently in both XeB- and vehicle-treated tumors (Figure 7D), consistent with the idea that tumor cells remain committed to enter the cell cycle, even when in a state of compromised bioenergetics caused by inhibition of $InsP_3R$ activity.

DISCUSSION

The main result of the present study is the demonstration of a unique requirement of tumorigenic cancer cells for constitutive ER-to-mitochondria Ca^{2+} transfer for their survival. In the absence of this transfer, either as a consequence of blocking $InsP_3R$-mediated Ca^{2+} release or blocking mitochondrial Ca^{2+} uptake, all tumor cells examined experienced a bioenergetic crisis similar to that of normal cells, but activation of autophagy, which enabled normal cells to survive, was insufficient, and the tumor cells died by necrosis as they proceeded through mitosis. Specific cancer cell killing was observed in human tumorigenic cell lines derived from breast, prostate, and cervix (HeLa), as well as, in data not shown, bone (143B), colon (SW480 and Colo320), kidney (RCCC), skin (WM3918, A231, WM239a, and B16F10), and brain (T98G) cancers. In addition, the same effect was observed in isogenic primary human fibroblasts transformed by expression of oncogenic Ras and enforced expression of Cdk4, a relevant combination found in spontaneous human cancers (Ridky et al., 2010). Furthermore, inhibition of $InsP_3R$ activity had strong anti-tumor efficacy in vivo.

Increased $InsP_3R$ expression and/or activity has been associated with cancer cell proliferation, growth, survival, and migration (Davis et al., 2013; Kang et al., 2010; Messai et al., 2014; Shibao et al., 2010; Szatkowski et al., 2010). Furthermore, MCU is highly expressed in ER-negative and basal-like breast cancers (Sørlie et al., 2006). Our results suggest that the fatal fate of cancer cells after $InsP_3R$ inhibition is a result of mitochondrial dysfunction, but it is independent of apoptotic mechanisms and, instead, appears linked to metabolic defects. Constitutive $InsP_3R$-mediated Ca^{2+} release is essential to support activity of PDH, a key enzyme that controls the flux of carbon into the TCA cycle, through Ca^{2+} activated PDH phosphatase activity. Consequently, diminished TCA production of NADH leads to

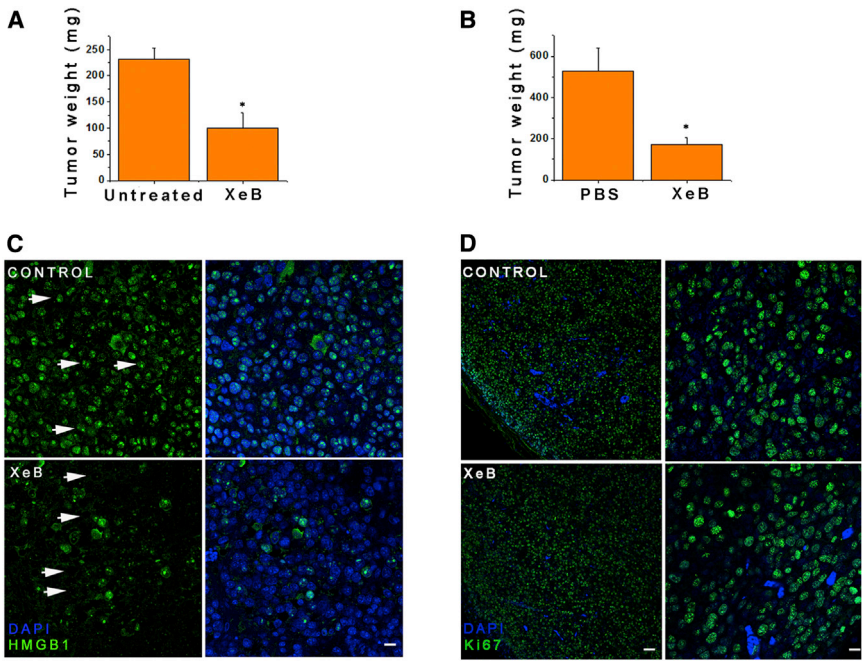

Figure 7. Inhibition of $InsP_3R$ Retards Tumor Growth In Vivo

Tumors were generated by subcutaneous injection of murine-melanoma-derived B16F10 cells into nude mice.

(A) Tumor weight in mice with tumors injected with 100 μl of a 100-μM XeB solution 1 day before euthanization. n = 9, mean ± SEM. *p < 0.05 (Student's t test).

(B) Tumor weight in mice with tumors injected with 100 μl of a 100-μM XeB solution or vehicle every other day for 6 days before euthanization. n = 9, mean ± SEM. *p < 0.05 (Student's t test).

(C) HMGB1 immunofluorescence in tumors injected, or not injected, with 100 μl of a 100-μM XeB solution 1 day before euthanization. The control tumor shows strong nuclear labeling (arrows), while in the XeB-treated tumor, the nuclei appear empty (arrows), with remaining labeling cytosolic or extracellular. n = 3. Scale bar represents 10 μm.

(D) Ki67 immunofluorescence in tumors injected, or not injected, with 100 μl of a 100-μM XeB solution 1 day before euthanization. Left: panoramic view of control and XeB-treated tumors. Scale bar represents 100 μm. Right: detail of control and XeB-treated tumors. Scale bar represents 10 μm. n = 3.

See also Figure S6.

lower rates of OXPHOS and a decline in ATP levels (Cárdenas et al., 2010). It is now recognized that most cancer cells rely on mitochondrial metabolism and use a significant fraction of glucose-derived pyruvate for ATP generation and for anaplerotic reactions to replenish TCA-cycle precursors for macromolecular biosynthesis (Ahn and Metallo, 2015; Jose et al., 2011; Koppenol et al., 2011; Moreno-Sánchez et al., 2007; Porporato et al., 2014). OXPHOS is important for ATP production in many cancers (Vander Heiden, 2013). Pancreatic cancer (Viale et al., 2014) and leukemic (Lagadinou et al., 2013; Nakada et al., 2010; Shi et al., 2012; Skrtić et al., 2011; Yang et al., 2011) stem cells, diffuse large B cell tumors (Caro et al., 2012), and primary glioblastoma sphere cultures (Janiszewska et al., 2012) rely on OXPHOS for survival. Primary human glioblastomas oxidize glucose via PDH and the TCA cycle during aggressive tumor growth (Marin-Valencia et al., 2012). Inhibition of complex 1 inhibits respiration and human cancer cell growth (Wheaton et al., 2014). The TCA cycle is also critically important in cancer cells for the generation of biochemical intermediates to sustain high rates of proliferation (Deberardinis et al., 2008). Most cancer cells derive lipogenic acetyl-coenzyme A (CoA) from pyruvate through Ca^{2+}-dependent PDH (Hatzivassiliou et al., 2005; Metallo et al., 2012), and activation of PDH can promote cancer cell senescence (Kaplon et al., 2013). Some cancers have defective OXPHOS but, nevertheless, rely on the TCA cycle (Mullen et al., 2012, 2014). Even in cancer cells with mutations in the TCA cycle, the turnover of TCA cycle intermediates is maintained (Mullen et al., 2012). Most cancer cells use PDH as well as glutamine to fuel the TCA cycle (DeBerardinis et al., 2007), where it enters and then cycles through α-KGDH as the first step (Mullen et al., 2014). Importantly, α-KGDH activity is strongly Ca^{2+} dependent (Armstrong et al., 2014), with apparent affinity similar to that of PDH phosphatase, suggesting that it may also be reduced by interruption of ER-to-mitochondria Ca^{2+} transfer. Reductive carboxylation of α-KG is observed in many cancer cells with impaired OXPHOS, where it maintains levels of biosynthetic intermediates. Notably, reductive carboxylation of α-KG requires its oxidation by Ca^{2+}-dependent α-KGDH (Mullen et al., 2014). Furthermore, reduction of α-KG to isocitrate is mediated by IDH, the other Ca^{2+} dependent enzyme in the TCA cycle. It is of interest that nucleotide supplementation prevented cancer cell death. α-KG is a precursor for glutamine and aspartate necessary for pyrimidine synthesis that requires mitochondrial dihydrooroate, which, in turn, requires flux through the electron transport chain (Grassian et al., 2014; Mullen et al., 2014). Together, these data suggest that cancer cells, by virtue of their reliance on OXPHOS and the TCA cycle for their viability, have a fundamental reliance on ER-to-mitochondria Ca^{2+} transfer via activation of Ca^{2+}-dependent dehydrogenases that fuel key steps in the TCA cycle and OXPHOS.

Normal cells also rely on OXPHOS and the TCA cycle, but, unlike the cancer cells examined, interruption of constitutive ER-to-mitochondria Ca^{2+} transfer had little effect on their viability, in agreement with previous observations (Cárdenas et al., 2010). Normal cells activate autophagy as a pro-survival mechanism under these conditions. The tumor cells also activated autophagy, and its inhibition tended to accelerate their cell death. What then distinguishes tumorigenic cells from non-tumorigenic cells that leads to mitochondrial Ca^{2+} addiction, specifically in cancer cells? Inhibition of mitochondrial Ca^{2+} uptake in non-tumorigenic cells slowed proliferation, whereas it didn't in the tumor cell lines. $InsP_3$-mediated Ca^{2+} signaling is important in cell-cycle progression (Ciapa et al., 1994; Han et al., 1992; Miller et al., 1993; Resende et al., 2010). Conversely, its inhibition

activates AMPK (Cárdenas et al., 2010; and discussed in the present study), which can phosphorylate and activate p53 to induce $p21^{waf1/cip1}$-mediated cell-cycle arrest (Jones et al., 2005). In contrast, proliferation of the tumor cells examined here was not slowed by inhibition of $InsP_3$-mediated Ca^{2+} signaling. MCF7 and HeLa cells have mutations in Cdk9 and Cdkn2 (http://lincs.hms.harvard.edu/) that may enable them to bypass Ca^{2+}-regulated checkpoints. The human fibroblasts we used were transformed by introducing a constitutively active Cdk4 that phosphorylates Rb independent of Ca^{2+} signaling. Whereas several of the cancer cell lines have mutated p53 that could explain lack of cell-cycle arrest in response to AMPK activation by $InsP_3R$ inhibition, we examined a broad collection of cell lines with normal and mutated p53 (http://p53.free.fr/index.html), and they all displayed uninhibited cell-cycle progression. Indeed, MCF7 and HeLa cells and transformed human fibroblasts that were used for most of our studies express wild-type p53. Although AMPK can suppress the mTOR pathway, which plays a role in coordinating cell growth and the cell cycle (Cuyàs et al., 2014), AMPK activation induced by $InsP_3R$ inhibition does not affect mTOR activity (Cárdenas et al., 2010). Thus, it remains unclear why proliferation was not reduced in tumorigenic cells in response to inhibition of $InsP_3R$ activity. Importantly, progression into mitosis resulted in catastrophic cell death during cytokinesis of all the tumor cells examined. Necrosis as the mechanism of cell death was confirmed by biochemical and histological markers in the cell lines, primary cells, and solid tumors. In contrast, neither apoptosis nor autophagy, nor necroptosis, appeared to play significant roles. The mechanisms that lead to mitotic catastrophic cell death (Vitale et al., 2011) around the time of cytokinesis remain to be determined. Interactions of the cyclin-dependent kinase substrate CP110 with Ca^{2+}-binding proteins calmodulin or centrin are essential for correct cytokinesis. Whereas the presence of a CP110 mutant unable to bind calmodulin induces cytokinesis failure and multinucleated cells (Tsang et al., 2006), it is possible that cytokinesis failure in the face of a bioenergetic crisis results, instead, in necrotic mitotic catastrophe. The failure of the tumorigenic cells to slow cell proliferation, despite the fact that they were in an energetically compromised state, appears to be the major mechanism that distinguishes them from non-tumorigenic cells and accounts for their susceptibility to cell killing.

In conclusion, using a variety of different tumorigenic cell lines and isogenic primary transformed human fibroblasts, we have demonstrated that constitutive $InsP_3R$-mediated Ca^{2+} transfer to mitochondria is essential in maintaining the viability of cancer cells. In the absence of this signal, normal cells restrict their entry into the cell cycle, whereas cancer cells bypass the Ca^{2+} checkpoints and undergo a catastrophic necrotic collapse during cytokinesis. Our results reveal a unique mitochondrial addiction to Ca^{2+} and a susceptibility of cancer cells that may have therapeutic implications.

EXPERIMENTAL PROCEDURES

Reagents

Antibodies were provided as follows. From Cell Signaling Technology: Phospho-α1-AMPK (Thr172), α1-AMPK, LC3B, HMBG1, ATG7, and caspase-3. From BD Biosciences: β-tubulin and $InsP_3R3$. From Sigma: MCU. $InsP_3R1$ antibody was provided by Dr. R.W. Neumar (University of Michigan). Secondary antibodies were conjugated with peroxidase from Amersham Biosciences. Chemicals: 3-methyladenine, methyl-pyruvate, dimethyl 2-oxoglutarate, FCCP, oligomycin, rotenone, and Hanks' balanced salt solution were purchased from Sigma. Z-VAD-FMK and necrostatin-1 were from Tocris Bioscience. U73122 and U73343 were from Calbiochem. TOTO-3, DAPI, cleaved caspase-3 conjugated with FITC, and secondary antibodies conjugated with Alexa Fluor 488 were from Molecular Probes. Xestospongin B was extracted and purified from the marine sponge *Xestospongia exigua* as described previously (Cárdenas et al., 2005).

Cell Culture and Transfection

Details regarding cell culture and transfection are available in the Supplemental Information.

Western Blotting and Treatments

Details of western blotting and cell treatments are available in the Supplemental Information.

Microscopy

Details of microscopy are available in the Supplemental Information.

Oxygen Consumption

OCR was measured at 37°C using an XF24 extracellular analyzer (Seahorse Bioscience). Details are provided in the Supplemental Information.

Clonogenic Assay

Colony formation was assayed as described previously (Franken et al., 2006) with details provided in the Supplemental Information.

Cell Cycle Analysis

Details are provided in the Supplemental Information.

Cell Death

Cell death was determined by LDH activity release by a colorimetric assay according to the manufacturer's instructions (Roche) and by PI (final concentration, 2.5 μg/ml) exclusion by flow cytometry (BD FACSCanto, BD Biosciences).

Mouse Tumor Generation and Histochemistry

All in vivo experiments were conducted with the approval of the University of Pennsylvania Institutional Animal Care and Use Committee. Murine-melanoma-derived B16F10 cells (1×10^5 cells) were subcutaneously injected into flanks of immunodeficient mice, and after 1 week, visible tumors were observed. Tumors of one flank were injected with 100 μl of a 100-μM XeB solution, and those on the contralateral side were left untreated or injected with 1% EtOH in PBS. Mice were euthanized after 1 day or 6 days of treatment with XeB, and tumors were extracted, weighed, and processed for immunohistochemistry.

Lactate Measurements

Cell lactate was measured colorometrically (Abcam) according to the manufacturer's instructions.

Glucose Uptake

Fibroblasts were washed with Krebs-BSA buffer, pre-incubated (or not) with cytochalasin B (10 min), and incubated for 10 min at 37°C with 10 mM ^{3}H-2-deoxyglucose. The reaction was stopped by placing it on ice, and the samples were spun, decanted, lysed in 1% Triton X-100, and cell ^{3}H quantified.

Analysis and Statistics

All data are summarized as means ± SEM; significance of differences was assessed using unpaired Student's t tests. Differences were accepted as significant at the 95% level ($p < 0.05$).

SUPPLEMENTAL INFORMATION

Supplemental Information includes Supplemental Experimental Procedures, six figures, and three movies and can be found with this article online at http://dx.doi.org/10.1016/j.celrep.2016.02.030.

AUTHOR CONTRIBUTIONS

C.C. and J.K.F. developed the hypotheses, designed experiments, and wrote the manuscript. C.C., M.M., A.M., A.L., F.J., F.U., G.B., and N.S. contributed to experimental design and data collection. J.M. provided the purified Xestospongin B. J.A.D. provided cell lines and guidance in nude mice experimental design. T.W.R. provided normal and transformed primary human fibroblasts.

ACKNOWLEDGMENTS

We thank Dr. Chi Van Dang for helpful discussions and comments. This work was supported by NIH grants R37GM56328 (J.K.F.), R01CA163566 (T.W.R.), R01CA133154 (J.A.D.), and P30NS047243 (A.L.), FONDECYT no. 1120443 (C.C.), FONDAP no. 15150012 (C.C.), and FONDECYT postdoctoral fellowship no. 3140458 (F.J.).

Received: July 15, 2015
Revised: December 24, 2015
Accepted: February 1, 2016
Published: March 3, 2016

REFERENCES

Ahn, C.S., and Metallo, C.M. (2015). Mitochondria as biosynthetic factories for cancer proliferation. Cancer Metab. *3*, 1.

Andrae, U., Singh, J., and Ziegler-Skylakakis, K. (1985). Pyruvate and related alpha-ketoacids protect mammalian cells in culture against hydrogen peroxide-induced cytotoxicity. Toxicol. Lett. *28*, 93–98.

Armstrong, C.T., Anderson, J.L., and Denton, R.M. (2014). Studies on the regulation of the human E1 subunit of the 2-oxoglutarate dehydrogenase complex, including the identification of a novel calcium-binding site. Biochem. J. *459*, 369–381.

Bayley, J.P., and Devilee, P. (2010). Warburg tumours and the mechanisms of mitochondrial tumour suppressor genes. Barking up the right tree? Curr. Opin. Genet. Dev. *20*, 324–329.

Birsoy, K., Possemato, R., Lorbeer, F.K., Bayraktar, E.C., Thiru, P., Yucel, B., Wang, T., Chen, W.W., Clish, C.B., and Sabatini, D.M. (2014). Metabolic determinants of cancer cell sensitivity to glucose limitation and biguanides. Nature *508*, 108–112.

Boroughs, L.K., and DeBerardinis, R.J. (2015). Metabolic pathways promoting cancer cell survival and growth. Nat. Cell Biol. *17*, 351–359.

Cárdenas, C., Liberona, J.L., Molgó, J., Colasante, C., Mignery, G.A., and Jaimovich, E. (2005). Nuclear inositol 1,4,5-trisphosphate receptors regulate local Ca^{2+} transients and modulate cAMP response element binding protein phosphorylation. J. Cell Sci. *118*, 3131–3140.

Cárdenas, C., Miller, R.A., Smith, I., Bui, T., Molgó, J., Müller, M., Vais, H., Cheung, K.H., Yang, J., Parker, I., et al. (2010). Essential regulation of cell bioenergetics by constitutive $InsP_3$ receptor Ca^{2+} transfer to mitochondria. Cell *142*, 270–283.

Caro, P., Kishan, A.U., Norberg, E., Stanley, I.A., Chapuy, B., Ficarro, S.B., Polak, K., Tondera, D., Gounarides, J., Yin, H., et al. (2012). Metabolic signatures uncover distinct targets in molecular subsets of diffuse large B cell lymphoma. Cancer Cell *22*, 547–560.

Cheng, G., Zielonka, J., Dranka, B.P., McAllister, D., Mackinnon, A.C., Jr., Joseph, J., and Kalyanaraman, B. (2012). Mitochondria-targeted drugs synergize with 2-deoxyglucose to trigger breast cancer cell death. Cancer Res. *72*, 2634–2644.

Ciapa, B., Pesando, D., Wilding, M., and Whitaker, M. (1994). Cell-cycle calcium transients driven by cyclic changes in inositol trisphosphate levels. Nature *368*, 875–878.

Cuyàs, E., Corominas-Faja, B., Joven, J., and Menendez, J.A. (2014). Cell cycle regulation by the nutrient-sensing mammalian target of rapamycin (mTOR) pathway. Methods Mol. Biol. *1170*, 113–144.

Davis, F.M., Parsonage, M.T., Cabot, P.J., Parat, M.O., Thompson, E.W., Roberts-Thomson, S.J., and Monteith, G.R. (2013). Assessment of gene expression of intracellular calcium channels, pumps and exchangers with epidermal growth factor-induced epithelial-mesenchymal transition in a breast cancer cell line. Cancer Cell Int. *13*, 76.

DeBerardinis, R.J., Mancuso, A., Daikhin, E., Nissim, I., Yudkoff, M., Wehrli, S., and Thompson, C.B. (2007). Beyond aerobic glycolysis: transformed cells can engage in glutamine metabolism that exceeds the requirement for protein and nucleotide synthesis. Proc. Natl. Acad. Sci. USA *104*, 19345–19350.

Deberardinis, R.J., Sayed, N., Ditsworth, D., and Thompson, C.B. (2008). Brick by brick: metabolism and tumor cell growth. Curr. Opin. Genet. Dev. *18*, 54–61.

Desler, C., Lykke, A., and Rasmussen, L.J. (2010). The effect of mitochondrial dysfunction on cytosolic nucleotide metabolism. J. Nucleic Acids *2010*, 701518.

Foskett, J.K., and Philipson, B. (2015). The mitochondrial Ca^{2+} uniporter complex. J. Mol. Cell. Cardiol. *78*, 3–8.

Foskett, J.K., White, C., Cheung, K.H., and Mak, D.O. (2007). Inositol trisphosphate receptor Ca^{2+} release channels. Physiol. Rev. *87*, 593–658.

Franken, N.A., Rodermond, H.M., Stap, J., Haveman, J., and van Bree, C. (2006). Clonogenic assay of cells in vitro. Nat. Protoc. *1*, 2315–2319.

Glancy, B., and Balaban, R.S. (2012). Role of mitochondrial Ca^{2+} in the regulation of cellular energetics. Biochemistry *51*, 2959–2973.

Grassian, A.R., Parker, S.J., Davidson, S.M., Divakaruni, A.S., Green, C.R., Zhang, X., Slocum, K.L., Pu, M., Lin, F., Vickers, C., et al. (2014). IDH1 mutations alter citric acid cycle metabolism and increase dependence on oxidative mitochondrial metabolism. Cancer Res. *74*, 3317–3331.

Han, J.K., Fukami, K., and Nuccitelli, R. (1992). Reducing inositol lipid hydrolysis, Ins(1,4,5)P3 receptor availability, or Ca^{2+} gradients lengthens the duration of the cell cycle in Xenopus laevis blastomeres. J. Cell Biol. *116*, 147–156.

Hatzivassiliou, G., Zhao, F., Bauer, D.E., Andreadis, C., Shaw, A.N., Dhanak, D., Hingorani, S.R., Tuveson, D.A., and Thompson, C.B. (2005). ATP citrate lyase inhibition can suppress tumor cell growth. Cancer Cell *8*, 311–321.

Jaimovich, E., Mattei, C., Liberona, J.L., Cardenas, C., Estrada, M., Barbier, J., Debitus, C., Laurent, D., and Molgó, J. (2005). Xestospongin B, a competitive inhibitor of IP3-mediated Ca^{2+} signalling in cultured rat myotubes, isolated myonuclei, and neuroblastoma (NG108-15) cells. FEBS Lett. *579*, 2051–2057.

Janiszewska, M., Suvà, M.L., Riggi, N., Houtkooper, R.H., Auwerx, J., Clément-Schatlo, V., Radovanovic, I., Rheinbay, E., Provero, P., and Stamenkovic, I. (2012). Imp2 controls oxidative phosphorylation and is crucial for preserving glioblastoma cancer stem cells. Genes Dev. *26*, 1926–1944.

Jones, R.G., and Thompson, C.B. (2009). Tumor suppressors and cell metabolism: a recipe for cancer growth. Genes Dev. *23*, 537–548.

Jones, R.G., Plas, D.R., Kubek, S., Buzzai, M., Mu, J., Xu, Y., Birnbaum, M.J., and Thompson, C.B. (2005). AMP-activated protein kinase induces a p53-dependent metabolic checkpoint. Mol. Cell *18*, 283–293.

Jose, C., Bellance, N., and Rossignol, R. (2011). Choosing between glycolysis and oxidative phosphorylation: a tumor's dilemma? Biochim. Biophys. Acta *1807*, 552–561.

Kang, S.S., Han, K.S., Ku, B.M., Lee, Y.K., Hong, J., Shin, H.Y., Almonte, A.G., Woo, D.H., Brat, D.J., Hwang, E.M., et al. (2010). Caffeine-mediated inhibition of calcium release channel inositol 1,4,5-trisphosphate receptor subtype 3 blocks glioblastoma invasion and extends survival. Cancer Res. *70*, 1173–1183.

Kaplon, J., Zheng, L., Meissl, K., Chaneton, B., Selivanov, V.A., Mackay, G., van der Burg, S.H., Verdegaal, E.M., Cascante, M., Shlomi, T., et al. (2013). A key role for mitochondrial gatekeeper pyruvate dehydrogenase in oncogene-induced senescence. Nature *498*, 109–112.

Koppenol, W.H., Bounds, P.L., and Dang, C.V. (2011). Otto Warburg's contributions to current concepts of cancer metabolism. Nat. Rev. Cancer *11*, 325–337.

Lagadinou, E.D., Sach, A., Callahan, K., Rossi, R.M., Neering, S.J., Minhajuddin, M., Ashton, J.M., Pei, S., Grose, V., O'Dwyer, K.M., et al. (2013). BCL-2 inhibition targets oxidative phosphorylation and selectively eradicates quiescent human leukemia stem cells. Cell Stem Cell *12*, 329–341.

Levine, A.J., and Puzio-Kuter, A.M. (2010). The control of the metabolic switch in cancers by oncogenes and tumor suppressor genes. Science *330*, 1340–1344.

Mallilankaraman, K., Cárdenas, C., Doonan, P.J., Chandramoorthy, H.C., Irrinki, K.M., Golenár, T., Csordás, G., Madireddi, P., Yang, J., Müller, M., et al. (2012a). MCUR1 is an essential component of mitochondrial Ca^{2+} uptake that regulates cellular metabolism. Nat. Cell Biol. *14*, 1336–1343.

Mallilankaraman, K., Doonan, P., Cárdenas, C., Chandramoorthy, H.C., Müller, M., Miller, R., Hoffman, N.E., Gandhirajan, R.K., Molgó, J., Birnbaum, M.J., et al. (2012b). MICU1 is an essential gatekeeper for MCU-mediated mitochondrial Ca^{2+} uptake that regulates cell survival. Cell *151*, 630–644.

Marin-Valencia, I., Yang, C., Mashimo, T., Cho, S., Baek, H., Yang, X.L., Rajagopalan, K.N., Maddie, M., Vemireddy, V., Zhao, Z., et al. (2012). Analysis of tumor metabolism reveals mitochondrial glucose oxidation in genetically diverse human glioblastomas in the mouse brain in vivo. Cell Metab. *15*, 827–837.

McCormack, J.G., and Denton, R.M. (1979). The effects of calcium ions and adenine nucleotides on the activity of pig heart 2-oxoglutarate dehydrogenase complex. Biochem. J. *180*, 533–544.

Messai, Y., Noman, M.Z., Hasmim, M., Janji, B., Tittarelli, A., Boutet, M., Baud, V., Viry, E., Billot, K., Nanbakhsh, A., et al. (2014). ITPR1 protects renal cancer cells against natural killer cells by inducing autophagy. Cancer Res. *74*, 6820–6832.

Metallo, C.M., Gameiro, P.A., Bell, E.L., Mattaini, K.R., Yang, J., Hiller, K., Jewell, C.M., Johnson, Z.R., Irvine, D.J., Guarente, L., et al. (2012). Reductive glutamine metabolism by IDH1 mediates lipogenesis under hypoxia. Nature *481*, 380–384.

Miller, A.L., Fluck, R.A., McLaughlin, J.A., and Jaffe, L.F. (1993). Calcium buffer injections inhibit cytokinesis in Xenopus eggs. J. Cell Sci. *106*, 523–534.

Momose, I., Ohba, S., Tatsuda, D., Kawada, M., Masuda, T., Tsujiuchi, G., Yamori, T., Esumi, H., and Ikeda, D. (2010). Mitochondrial inhibitors show preferential cytotoxicity to human pancreatic cancer PANC-1 cells under glucose-deprived conditions. Biochem. Biophys. Res. Commun. *392*, 460–466.

Moreno-Sánchez, R., Rodríguez-Enríquez, S., Marín-Hernández, A., and Saavedra, E. (2007). Energy metabolism in tumor cells. FEBS J. *274*, 1393–1418.

Mullen, A.R., Wheaton, W.W., Jin, E.S., Chen, P.H., Sullivan, L.B., Cheng, T., Yang, Y., Linehan, W.M., Chandel, N.S., and DeBerardinis, R.J. (2012). Reductive carboxylation supports growth in tumour cells with defective mitochondria. Nature *481*, 385–388.

Mullen, A.R., Hu, Z., Shi, X., Jiang, L., Boroughs, L.K., Kovacs, Z., Boriack, R., Rakheja, D., Sullivan, L.B., Linehan, W.M., et al. (2014). Oxidation of alpha-ketoglutarate is required for reductive carboxylation in cancer cells with mitochondrial defects. Cell Rep. *7*, 1679–1690.

Munshi, A., Hobbs, M., and Meyn, R.E. (2005). Clonogenic cell survival assay. Methods Mol. Med. *110*, 21–28.

Murphy, A.N., Kelleher, J.K., and Fiskum, G. (1990). Submicromolar Ca^{2+} regulates phosphorylating respiration by normal rat liver and AS-30D hepatoma mitochondria by different mechanisms. J. Biol. Chem. *265*, 10527–10534.

Nakada, D., Saunders, T.L., and Morrison, S.J. (2010). Lkb1 regulates cell cycle and energy metabolism in haematopoietic stem cells. Nature *468*, 653–658.

Porporato, P.E., Payen, V.L., Pérez-Escuredo, J., De Saedeleer, C.J., Danhier, P., Copetti, T., Dhup, S., Tardy, M., Vazeille, T., Bouzin, C., et al. (2014). A mitochondrial switch promotes tumor metastasis. Cell Rep. *8*, 754–766.

Resende, R.R., Adhikari, A., da Costa, J.L., Lorençon, E., Ladeira, M.S., Guatimosim, S., Kihara, A.H., and Ladeira, L.O. (2010). Influence of spontaneous calcium events on cell-cycle progression in embryonal carcinoma and adult stem cells. Biochim. Biophys. Acta *1803*, 246–260.

Ridky, T.W., Chow, J.M., Wong, D.J., and Khavari, P.A. (2010). Invasive three-dimensional organotypic neoplasia from multiple normal human epithelia. Nat. Med. *16*, 1450–1455.

Scaffidi, P., Misteli, T., and Bianchi, M.E. (2002). Release of chromatin protein HMGB1 by necrotic cells triggers inflammation. Nature *418*, 191–195.

Shi, Y., Dierckx, A., Wanrooij, P.H., Wanrooij, S., Larsson, N.G., Wilhelmsson, L.M., Falkenberg, M., and Gustafsson, C.M. (2012). Mammalian transcription factor A is a core component of the mitochondrial transcription machinery. Proc. Natl. Acad. Sci. USA *109*, 16510–16515.

Shibao, K., Fiedler, M.J., Nagata, J., Minagawa, N., Hirata, K., Nakayama, Y., Iwakiri, Y., Nathanson, M.H., and Yamaguchi, K. (2010). The type III inositol 1,4,5-trisphosphate receptor is associated with aggressiveness of colorectal carcinoma. Cell Calcium *48*, 315–323.

Skrtić, M., Sriskanthadevan, S., Jhas, B., Gebbia, M., Wang, X., Wang, Z., Hurren, R., Jitkova, Y., Gronda, M., Maclean, N., et al. (2011). Inhibition of mitochondrial translation as a therapeutic strategy for human acute myeloid leukemia. Cancer Cell *20*, 674–688.

Sørlie, T., Wang, Y., Xiao, C., Johnsen, H., Naume, B., Samaha, R.R., and Børresen-Dale, A.L. (2006). Distinct molecular mechanisms underlying clinically relevant subtypes of breast cancer: gene expression analyses across three different platforms. BMC Genomics *7*, 127.

Szatkowski, C., Parys, J.B., Ouadid-Ahidouch, H., and Matifat, F. (2010). Inositol 1,4,5-trisphosphate-induced Ca^{2+} signalling is involved in estradiol-induced breast cancer epithelial cell growth. Mol. Cancer *9*, 156.

Territo, P.R., Mootha, V.K., French, S.A., and Balaban, R.S. (2000). Ca^{2+} activation of heart mitochondrial oxidative phosphorylation: role of the F(0)/F(1)-ATPase. Am. J. Physiol. Cell Physiol. *278*, C423–C435.

Tsang, W.Y., Spektor, A., Luciano, D.J., Indjeian, V.B., Chen, Z., Salisbury, J.L., Sánchez, I., and Dynlacht, B.D. (2006). CP110 cooperates with two calcium-binding proteins to regulate cytokinesis and genome stability. Mol. Biol. Cell *17*, 3423–3434.

Vander Heiden, M.G. (2013). Exploiting tumor metabolism: challenges for clinical translation. J. Clin. Invest. *123*, 3648–3651.

Vander Heiden, M.G., Cantley, L.C., and Thompson, C.B. (2009). Understanding the Warburg effect: the metabolic requirements of cell proliferation. Science *324*, 1029–1033.

Viale, A., Pettazzoni, P., Lyssiotis, C.A., Ying, H., Sánchez, N., Marchesini, M., Carugo, A., Green, T., Seth, S., Giuliani, V., et al. (2014). Oncogene ablation-resistant pancreatic cancer cells depend on mitochondrial function. Nature *514*, 628–632.

Vitale, I., Galluzzi, L., Castedo, M., and Kroemer, G. (2011). Mitotic catastrophe: a mechanism for avoiding genomic instability. Nat. Rev. Mol. Cell Biol. *12*, 385–392.

Warburg, O. (1956). On the origin of cancer cells. Science *123*, 309–314.

Wheaton, W.W., Weinberg, S.E., Hamanaka, R.B., Soberanes, S., Sullivan, L.B., Anso, E., Glasauer, A., Dufour, E., Mutlu, G.M., Budigner, G.S., and Chandel, N.S. (2014). Metformin inhibits mitochondrial complex I of cancer cells to reduce tumorigenesis. eLife *3*, e02242.

Wise, D.R., and Thompson, C.B. (2010). Glutamine addiction: a new therapeutic target in cancer. Trends Biochem. Sci. *35*, 427–433.

Yang, S., Wang, X., Contino, G., Liesa, M., Sahin, E., Ying, H., Bause, A., Li, Y., Stommel, J.M., Dell'antonio, G., et al. (2011). Pancreatic cancers require autophagy for tumor growth. Genes Dev. *25*, 717–729.

Zhang, X., Fryknäs, M., Hernlund, E., Fayad, W., De Milito, A., Olofsson, M.H., Gogvadze, V., Dang, L., Påhlman, S., Schughart, L.A., et al. (2014). Induction of mitochondrial dysfunction as a strategy for targeting tumour cells in metabolically compromised microenvironments. Nat. Commun. *5*, 3295.

Cell Reports, Volume *14*

Supplemental Information

Selective Vulnerability of Cancer Cells by Inhibition of Ca^{2+} Transfer from Endoplasmic Reticulum to Mitochondria

César Cárdenas, Marioly Müller, Andrew McNeal, Alenka Lovy, Fabian Jaňa, Galdo Bustos, Felix Urra, Natalia Smith, Jordi Molgó, J. Alan Diehl, Todd W. Ridky, and J. Kevin Foskett

SUPPLEMENTARY INFORMATION

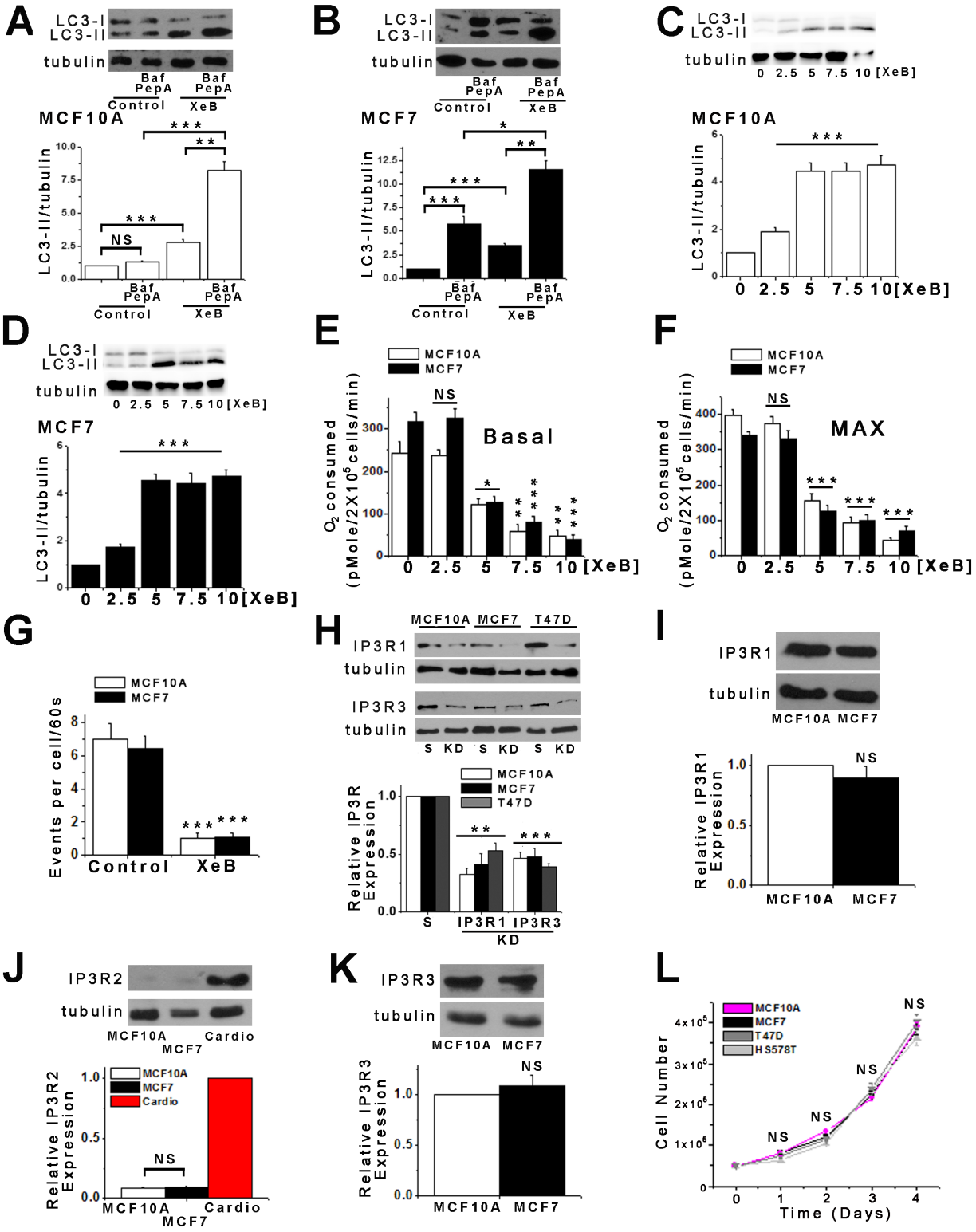

Figure S1

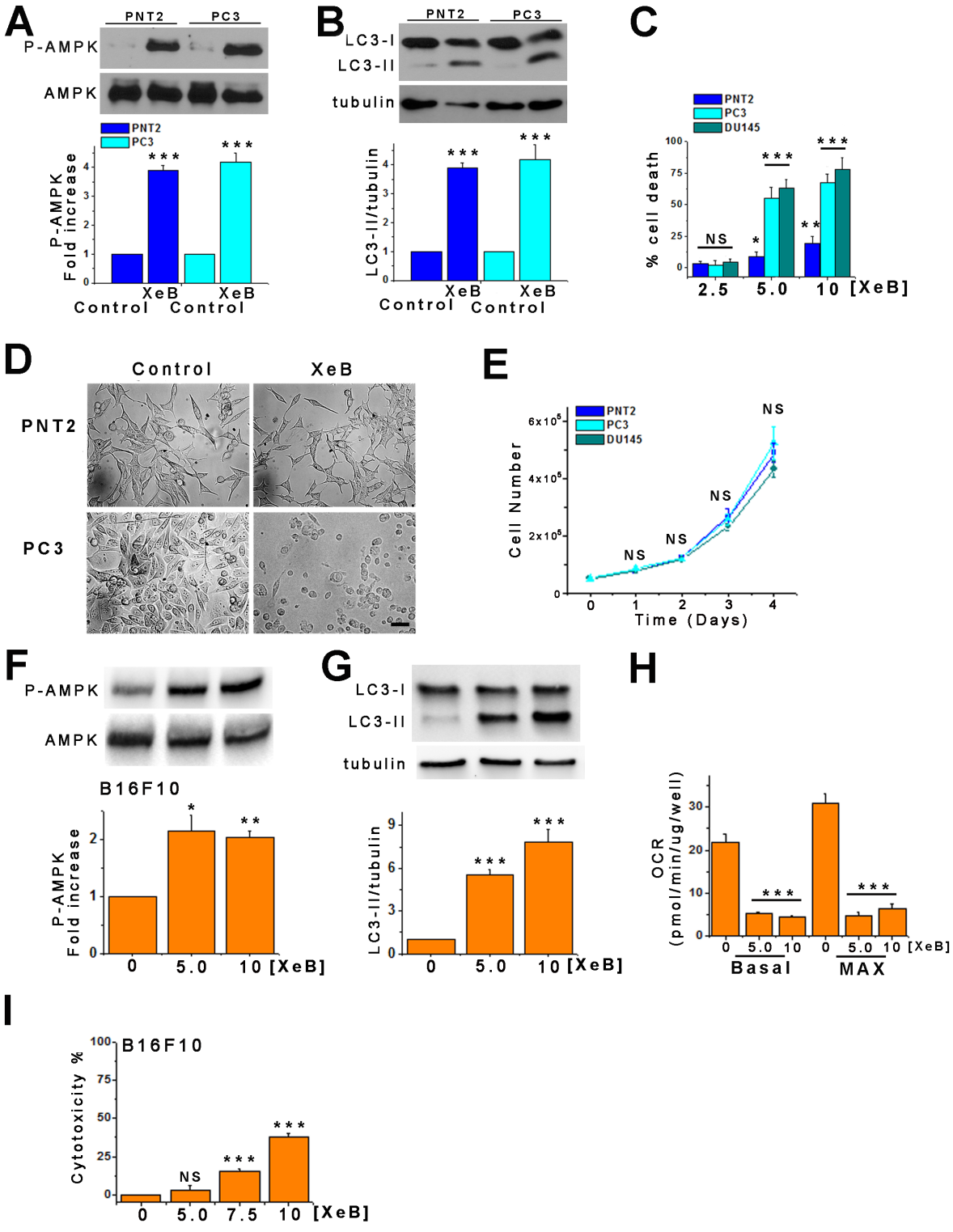
A
PNT2
PC3
P-AMPK
AMPK
PNT2
PC3
P-AMPK
Fold increase
***
***
Control
XeB
Control
XeB
B
PNT2
PC3
LC3-I
LC3-II
tubulin
LC3-II/tubulin
***
***
Control
XeB
Control
XeB
C
PNT2
PC3
DU145
% cell death
NS
*
***
**
***
2.5
5.0
10 [XeB]
D
Control
XeB
PNT2
PC3
E
PNT2
PC3
DU145
Cell Number
6x10^5
4x10^5
2x10^5
0
NS
NS
NS
NS
0
1
2
3
4
Time (Days)
F
P-AMPK
AMPK
B16F10
P-AMPK
Fold increase
*
**
0
5.0
10 [XeB]
G
LC3-I
LC3-II
tubulin
LC3-II/tubulin
***
***
0
5.0
10 [XeB]
H
OCR
(pmol/min/ug/well)
***
***
0
5.0
10 [XeB]
0
5.0
10 [XeB]
Basal
MAX
I
B16F10
Cytotoxicity %
NS
***
***
0
5.0
7.5
10 [XeB]

Figure S2

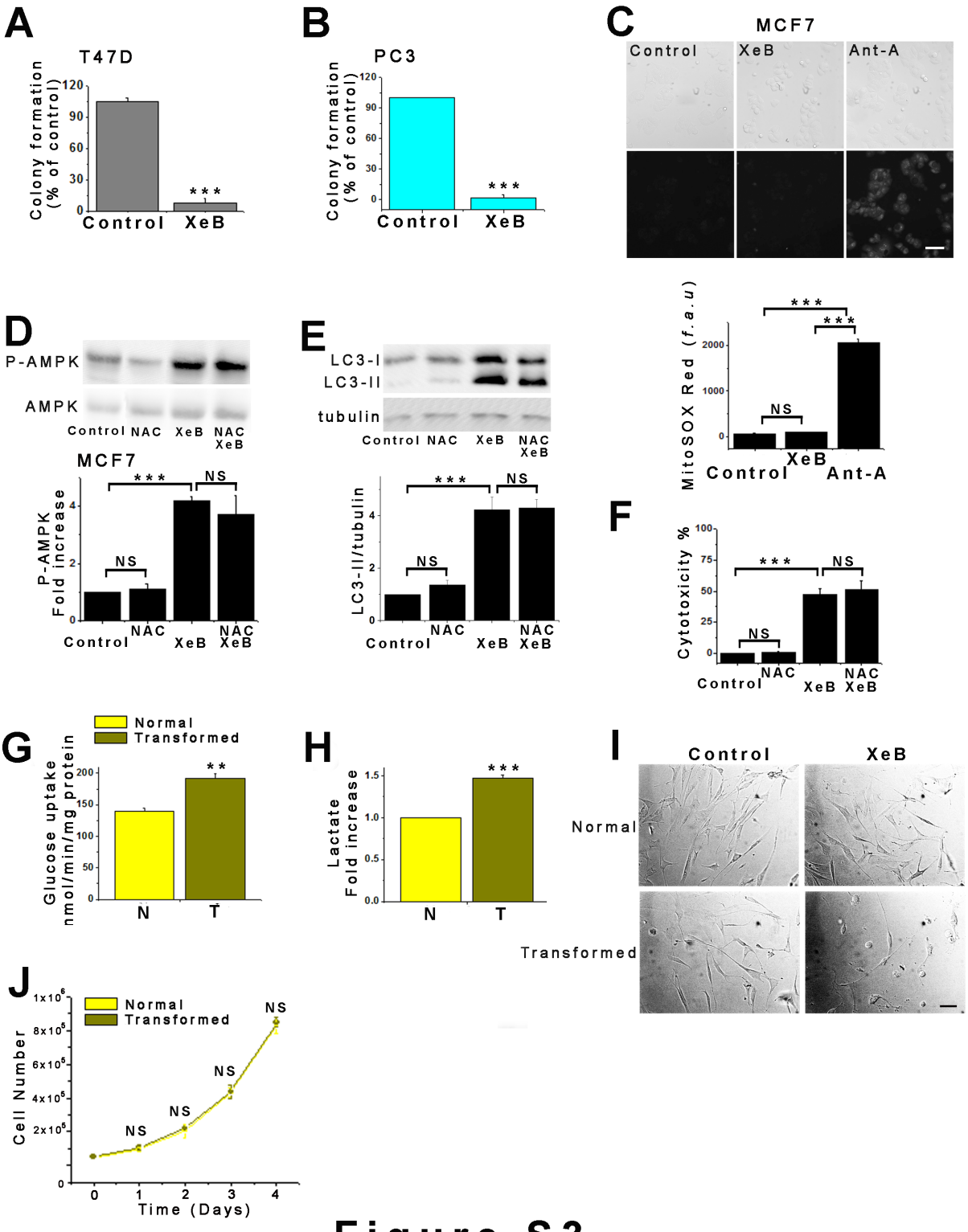
A
T47D
Colony formation (% of control)
120
90
60
30
0
***
Control
XeB
B
PC3
Colony formation (% of control)
120
90
60
30
0
***
Control
XeB
C
MCF7
Control
XeB
Ant-A
D
P-AMPK
AMPK
Control NAC XeB NAC XeB
MCF7
P-AMPK Fold increase
***
NS
NS
4
2
0
Control
NAC
XeB
NAC XeB
E
LC3-I
LC3-II
tubulin
Control NAC XeB NAC XeB
LC3-II/tubulin
***
NS
NS
4
2
0
Control
NAC
XeB
NAC XeB
MitoSOX Red (f.a.u)
***
***
NS
2000
1000
0
Control
XeB
Ant-A
F
Cytotoxicity %
***
NS
NS
100
75
50
25
0
Control
NAC
XeB
NAC XeB
G
Normal
Transformed
Glucose uptake nmol/min/mg protein
**
200
150
100
50
0
N
T
H
Lactate Fold increase
***
1.5
1.0
0.5
0.0
N
T
I
Control
XeB
Normal
Transformed
J
Normal
Transformed
Cell Number
1x10^6
8x10^5
6x10^5
4x10^5
2x10^5
0
NS
NS
NS
NS
0
1
2
3
4
Time (Days)

Figure S3

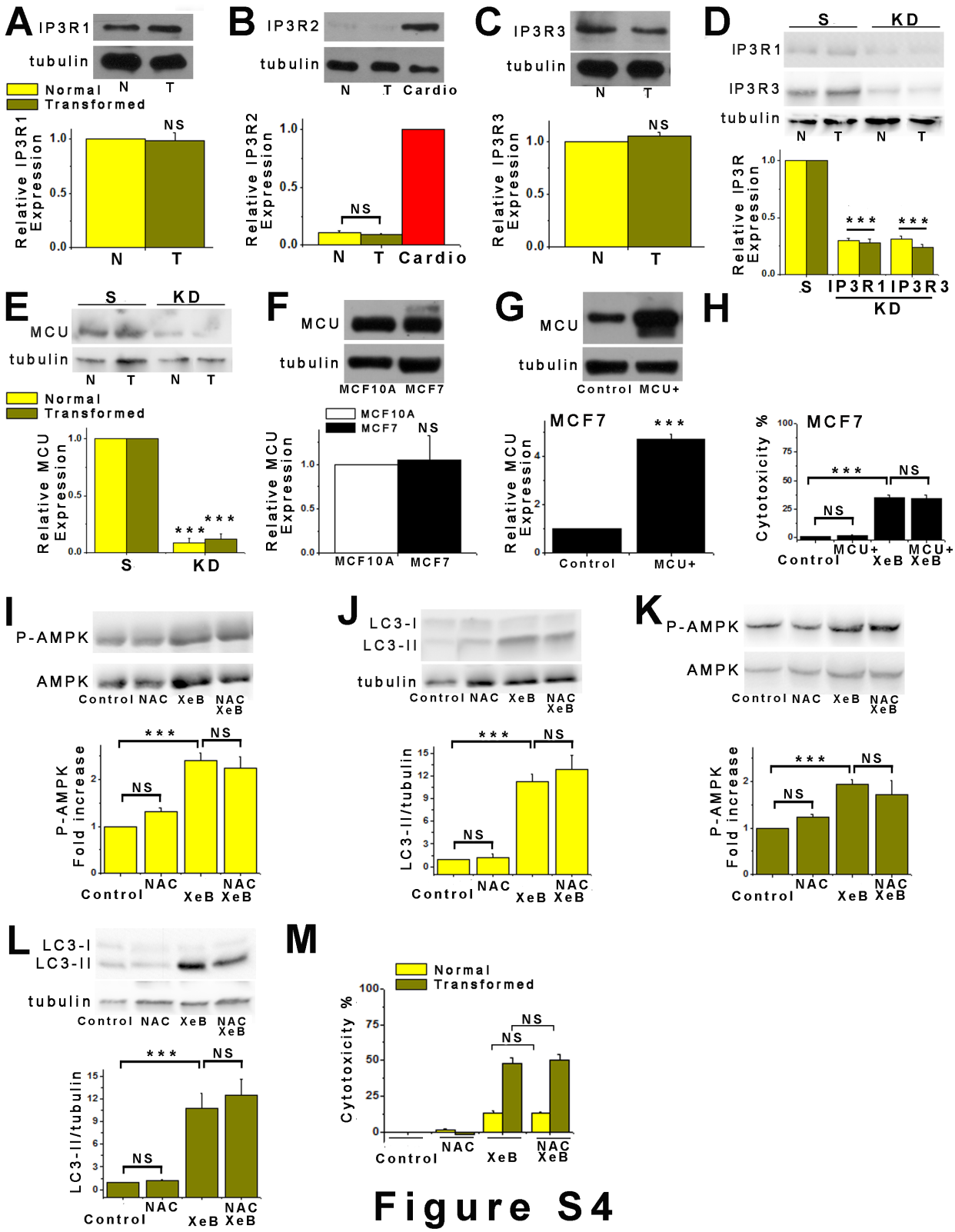
A
IP3R1
tubulin
N T
Normal
Transformed
Relative IP3R1 Expression
NS
B
IP3R2
tubulin
N T Cardio
Relative IP3R2 Expression
NS
C
IP3R3
tubulin
N T
Relative IP3R3 Expression
NS
D
S KD
IP3R1
IP3R3
tubulin
N T N T
Relative IP3R Expression
***
***
S IP3R1 IP3R3
KD
E
S KD
MCU
tubulin
N T N T
Normal
Transformed
Relative MCU Expression
***
***
S KD
F
MCU
tubulin
MCF10A MCF7
MCF10A
MCF7
NS
Relative MCU Expression
MCF10A MCF7
G
MCU
tubulin
Control MCU+
MCF7
***
Relative MCU Expression
Control MCU+
H
MCF7
Cytotoxicity %
***
NS
NS
Control MCU+ MCU+
XeB XeB
I
P-AMPK
AMPK
Control NAC XeB NAC XeB
***
NS
NS
P-AMPK Fold increase
Control NAC XeB NAC XeB
J
LC3-I
LC3-II
tubulin
Control NAC XeB NAC XeB
***
NS
NS
LC3-II/tubulin
Control NAC XeB NAC XeB
K
P-AMPK
AMPK
Control NAC XeB NAC XeB
***
NS
NS
P-AMPK Fold increase
Control NAC XeB NAC XeB
L
LC3-I
LC3-II
tubulin
Control NAC XeB NAC XeB
***
NS
NS
LC3-II/tubulin
Control NAC XeB NAC XeB
M
Normal
Transformed
Cytotoxicity %
NS
NS
Control NAC XeB NAC XeB

Figure S4

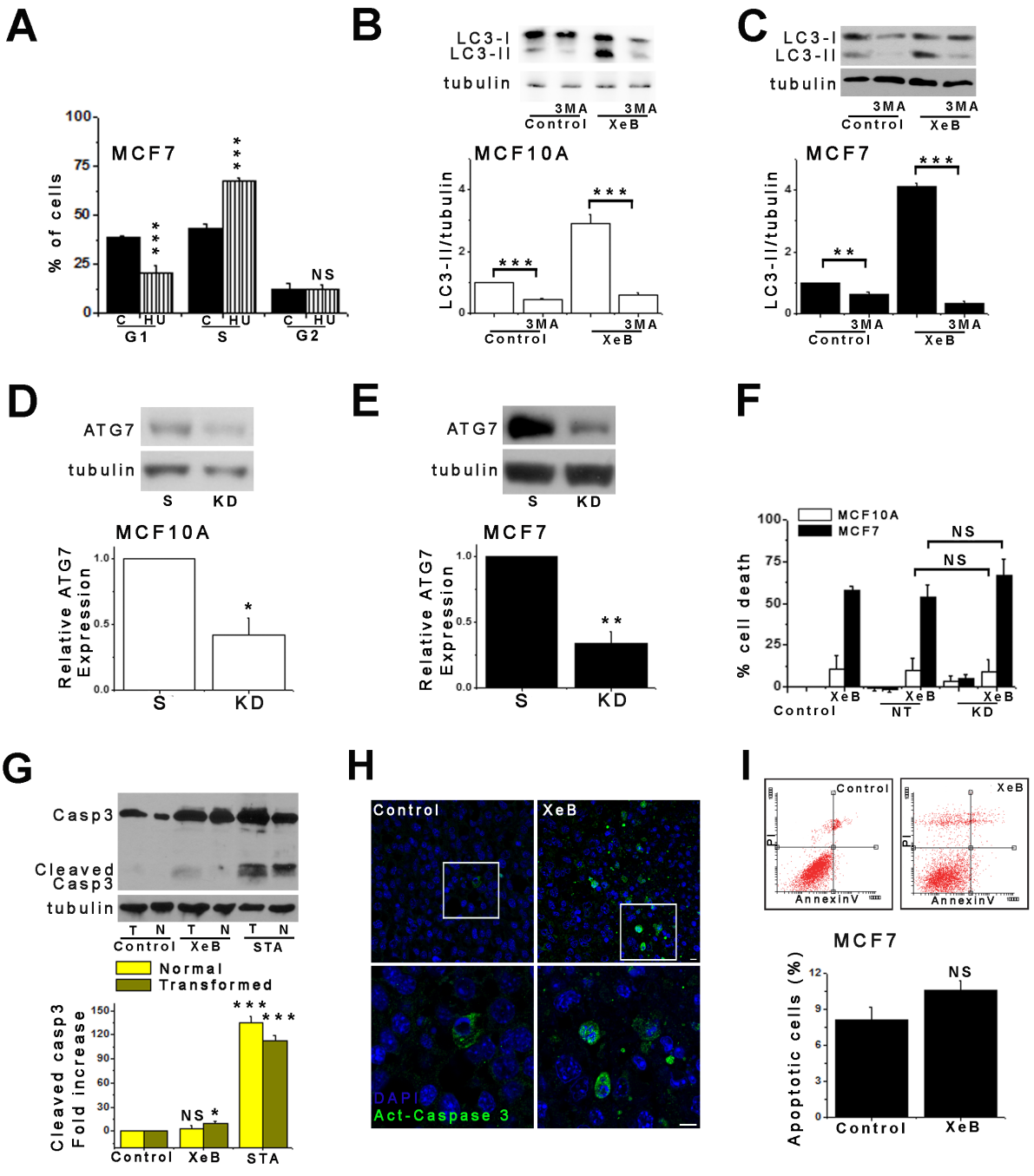
A
MCF7
% of cells
C HU
G1
S
G2
NS
B
LC3-I
LC3-II
tubulin
3MA
Control
XeB
MCF10A
LC3-II/tubulin
C
MCF7
D
ATG7
tubulin
S
KD
MCF10A
Relative ATG7 Expression
E
MCF7
F
MCF10A
MCF7
% cell death
Control
NT
KD
G
Casp3
Cleaved Casp3
T N
STA
Normal
Transformed
Cleaved casp3 Fold increase
H
Control
XeB
DAPI
Act-Caspase 3
I
PI
AnnexinV
Apoptotic cells (%)

Figure S5

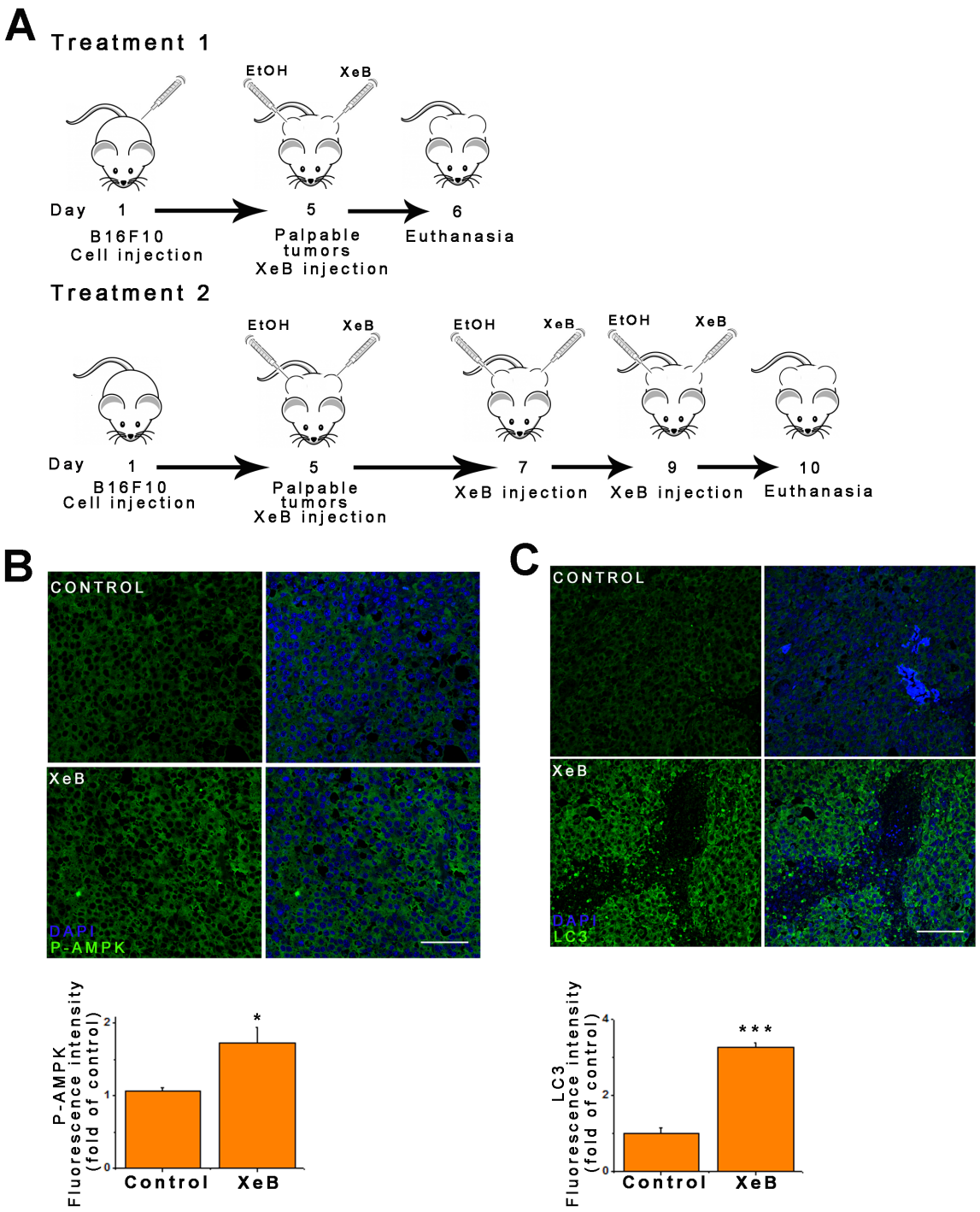
A
Treatment 1
EtOH
XeB
Day 1
B16F10
Cell injection
5
Palpable
tumors
XeB injection
6
Euthanasia
Treatment 2
EtOH
XeB
EtOH
XeB
EtOH
XeB
Day 1
B16F10
Cell injection
5
Palpable
tumors
XeB injection
7
XeB injection
9
XeB injection
10
Euthanasia
B
CONTROL
XeB
DAPI
P-AMPK
P-AMPK
Fluorescence intensity
(fold of control)
*
Control
XeB
C
CONTROL
XeB
DAPI
LC3
LC3
Fluorescence intensity
(fold of control)
***
Control
XeB

Figure S6

SUPPLEMENTARY FIGURE LEGENDS

Figure S1. Characterization of the $InsP_3R$ inhibitor XeB in Breast Cell Lines and the Expression of $InsP_3R$, related to Figure 1.

(A) Representative Westerns blots of autophagy marker LC3 or tubulin as loading control in MCF10A cell line treated with 5 μM XeB (1h) after a 6h incubation with bafilomycin A1 (Baf) and pepstatine A (PepA). Quantification of LC3-II/tubulin expressed as fold increase over basal levels (control cells). N=3, mean ± S.E., **p< 0.01, ***p<0.001, NS: not significant (t-test).

(B) As in (A) using MCF7 cell line. N=3, mean ± S.E., *p< 0.05, **p< 0.01, ***p<0.001 (t-test).

(C) Representative Westerns blots of autophagy marker LC3 or tubulin as loading control in MCF10A cell line treated with increasing concentrations of XeB (1 h) and quantification of LC3-II/tubulin expressed as fold increase over basal levels (control cells). N=3, mean ± S.E. ***p<0.001 (one-way analysis of variance followed by Dunnett's multiple comparison post-test).

(D) As in (C) using MCF7 cell line. N=3, mean ± S.E. ***p<0.001 (one-way analysis of variance followed by Dunnett's multiple comparison post-test).

(E) Basal oxygen consumption rates (OCR) of tumorigenic and normal breast cell lines MCF10A and MCF7 incubated with increasing concentrations of XeB for 1h. N=3, mean ± S.E., *p<0.05, **p<0.01 (t-test), ***p<0.001, NS: not significant (t-test).

(F) Maximum OCR of normal MCF10A and tumorigenic MCF7 breast cell lines incubated with increasing concentrations of XeB for 1 h. N=3, mean ± S.E., *p<0.05, **p<0.01 (t-test), ***p<0.001, NS: not significant (t-test).

(G) Quantification of spontaneous Ca^{2+} release events in MCF10A and MCF7 cells treated or not with XeB. 25 cells per experiment were analyzed. N=3, mean ± S.E., NS: not significant (t-test).

(H) Non-tumorigenic (MCF10A) and tumorigenic (MCF7, T47D) breast cells transiently transfected with a siRNA against type 1 and type 3 $InsP_3R$ or a scrambled non-target (S) siRNA for 24 hr. Bar graph: summary of expression. Protein expression was reduced by: MCF10A, type1; 67% ± 6%, type 3; 53% ± 5%; MCF7, type1; 59% ± 10%, type 3; 52% ± 7%; T47D, type1; 47% ± 7%, type 3; 61% ± 3%). N=3, mean ± S.E., **p<0.01, ***p < 0.001 (t-test).

(I) Representative Western blots of type 1 $InsP_3R$ (IP3R1) in non-tumorigenic (MCF10A) and tumorigenic (MCF7) breast cell lines and quantification of IP3R1/tubulin expressed as relative expression compared with MCF10A. N=3, mean ± S.E., NS: not significant (t-test).

(J) Representative Western blots of type 2 $InsP_3R$ (IP3R2) in non-tumorigenic (MCF10A) tumorigenic (MCF7) breast cell lines, and cardiomyocytes (Cardio) as a positive control. Quantification of IP3R2/tubulin expressed as relative expression compared with cardiomyocytes. N=3, mean ± S.E., NS: not significant (t-test).

(K) As in (I) for the type 3 $InsP_3R$ (IP3R3). N=3, mean ± S.E., NS: not significant (t-test).

(L) Growth curves of non-tumorigenic and tumorigenic breast cell lines. N=3, mean ± S.E., NS: not significant (t-test).

Figure S2. Inhibition of $InsP_3R$ Signaling in Human Prostate Cells and Mouse Melanoma Cells, related to Figure 2.

(A) Representative Western blots of phosphorylated (P-AMPK) and total AMPK in PNT2 (non-tumorigenic) and PC3 (tumorigenic) human prostate cells treated with 5 µM XeB for 1h. Bar graph: P-AMPK/AMPK expressed as average fold increase over basal levels (control cells). N=3, mean ± S.E. ***p<0.001 (t-test).

(B) Representative Western blots of autophagy marker LC3 or tubulin as loading control in PNT2 and PC3 cells treated with 5 µM XeB for 1h. Bar graph: quantification of LC3-II/tubulin expressed as average fold increase over basal levels (control cells). N=3, mean ± S.E., **p<0.01, ***p<0.001 (t-test).

(C) Non-tumorigenic (PNT2) and tumorigenic (PC3 and Du145) human-derived prostate cell lines were treated with increasing concentrations of XeB as indicated for 24h and cell death was determined by TOTO-3 incorporation by flow cytometry. N=3, mean ± S.E., *p<0.005, **p<0.01, *** p<0.001, NS: not significant (t-test).

(D) DIC images of normal (PNT2) or tumorigenic (PC3) cells treated with 5 µM XeB for 24h. Bar: 10 µm. N = 3.

(E) Growth curves of non-tumorigenic and tumorigenic prostate cell lines. N=3, mean ± S.E., NS: not significant (t-test).

(F) Representative Western blots of phosphorylated (P-AMPK) and total AMPK in B16F10 melanoma cells treated with 5 or 10 µM XeB for 1h. Bar graph: P-AMPK/AMPK expressed as average fold increase over basal levels (control cells). N=3, mean ± S.E., *p<0.05, **p<0.01 (t-test).

(G) Representative Western blots of autophagy marker LC3 and tubulin as loading control in B16F10 cells treated with 5 or 10 µM XeB for 1h. Bar graph: quantification of LC3-II/tubulin expressed as average fold increase over basal levels (control cells). N=3, mean ± S.E., ***p<0.001 (t test).

(H) Basal and maximum OCR of B16F10 cells incubated with 5 or 10 µM XeB for 1h. N=3, mean ± S.E., ***p<0.001 (t-test).

(I) Cell death determined by LDH release in cells treated with increasing concentrations of XeB as indicated. N=3, mean ± S.E, ***p<0.001, NS: not significant (t-test).

Figure S3. Inhibition of $InsP_3R$ Signaling Impairs Colony Formation Unrelated to Reactive Oxygen Species, and Metabolic Features of Primary Human Fibroblasts, related to Figures 3 and 4.

(A) Quantitative analysis of colony formation in tumorigenic T47D breast cell line treated or not with 5 µM XeB for 24h. N=3, mean ± S.E, ***p<0.001 (t-test).

(B) Same as in (A) in tumorigenic prostate PC3 cell line. N=3, mean ± S.E, ***p<0.001 (t-test).

(C) Top: Mitochondrial superoxide generation determined by MitoSOX red fluorescence in MCF7 cells treated with 5 µM XeB for 4h. 10 µM antimycin A (Ant-A) used as positive control. Bottom: Summary, N = 4, mean ± S.E,***p<0.001, NS: not significant (t-test).

(D) Representative Western blots of phosphorylated (P-AMPK) and total AMPK in MCF7 cells treated with 5 µM XeB for 1h in presence or absence of 5 mM n-acetylcysteine (NAC). Bar graph: P-AMPK/AMPK expressed as average fold increase over basal levels (control cells). N=3, mean ± S.E., ***p<0.001, NS: not significant (t-test).

(E) Representative Western blots of autophagy marker LC3 or tubulin as loading control in normal fibroblasts treated with 5 μM XeB for 1h in presence or absence of 5 mM n-acetylcysteine (NAC). Bar graph: quantification of LC3-II/tubulin expressed as average fold increase over basal levels (control cells). N=3, mean ± S.E., ***p<0.001 (t-test).

(F) MCF7 cells were treated with 5 μM XeB in absence or presence of 5 mM n-acetylcysteine (NAC) for 24 for and cell death was determined by LDH release. N=3, mean ± S.E., NS: not significant, ***p<0.001 (t test).

(G) Glucose uptake in normal and transformed human fibroblasts determined radiometrically by incorporation of ^{3}H-2-deoxyglucose (10 mM). N=3, mean ± S.E., **p<0.01 (t-test).

(H) Lactate generation in normal and transformed fibroblasts. N=3, mean ± S.E., ***p<0.001 (t-test).

(I) DIC images of normal and transformed fibroblasts treated with vehicle (control) or 5 μM XeB for 24h. Bar: 10 μm. N=3.

(J) Growth curves of normal and transformed fibroblasts. N=3, mean ± S.E., NS: not significant (t-test).

Figure S4. Physiological and Metabolic Features of Primary Human Fibroblasts, related to Figure 4.

(A) Representative Western blots of type 1 $InsP_3R$ (IP3R1) in normal (N) and transformed (T) cells and quantification of IP3R1/tubulin expressed as relative expression over the normal cells. N=3, mean ± S.E., NS: not significant (t-test).

(B) Representative Western blots of type 2 $InsP_3R$ (IP3R2) in normal (N) and transformed (T) cells, and cardiomyocytes (Cardio) as positive control. Quantification of IP3R2/tubulin expressed as relative expression over the cardiomyocytes. N=3, mean ± S.E., NS: not significant (t-test).

(C) As in (A) for the type 3 $InsP_3R$ (IP3R3). N=3, mean ± S.E., NS: not significant (t-test).

(D) Representative Western blots of types 1 and 3 $InsP_3R$ expression in normal (N) and transformed (T) fibroblasts treated or not with types 1 and 3 siRNA. Bar graph: quantification of InsP3R/tubulin expressed as relative expression to control levels in cells transfected with a scrambled non-targeting siRNA (S). $InsP_3R$ protein reduced by 70 ± 2% and 69 ± 3 % for types 1 and 3, respectively in normal cells; and by 72 ± 3% and 76 ± 2 %, respectively in transformed cells 48 h after transfection compared with cells transfected with non-targeting siRNA. N=3, mean ± S.E., ***p<0.001 (t-test).

(E) Representative Western blot of MCU expression in normal (N) and transformed (T) fibroblasts. Bar graph represents MCU/tubulin relative expression compared with cells transfected with a non-targeting scrambled siRNA (S). MCU protein was reduced by 91 ± 3 % in normal and 87 ± 4 % in transformed cells 72 h post transfection. N=3, mean ± S.E.,***p<0.001 (t-test).

(F) Representative Western blots of MCU in non-tumorigenic (MCF10A) and tumorigenic (MCF7) breast cell lines and quantification of MCU/tubulin expressed as relative expression over the MCF10A cells. N=3, mean ± S.E., NS: not significant (t-test).

(G) Representative Western blots of MCU in MCF7 cell line expressing either MCU (MCU+) or the empty vector as control. Quantification of MCU/tubulin expressed as relative expression over the control. N=3, mean ± S.E., ***p<0.001 (t-test).

(H) MCU expressing (MCU+) cells and control were treated with 5 µM XeB and cell death was determined by LDH release. N=3, mean ± S.E., ***p<0.001, NS: not significant (t-test).
(I) Representative Western blots of phosphorylated (P-AMPK) and total AMPK in normal fibroblasts treated with 5 µM XeB for 1h in presence or absence of 5 mM n-acetylcysteine (NAC). Bar graph: P-AMPK/AMPK expressed as average fold increase over basal levels (control cells). N=3, mean ± S.E., ***p<0.001, NS: not significant (t-test).
(J) Representative Western blots of autophagy marker LC3 and tubulin as loading control in normal fibroblasts treated with 5 µM XeB for 1h in presence or absence of 5mM n-acetylcysteine (NAC). Bar graph: quantification of LC3-II/tubulin expressed as average fold increase over basal levels (control cells). N=3, mean ± S.E., ***p<0.001, NS: not significant (t-test).
(K) Representative Western blots of phosphorylated (P-AMPK) and total AMPK in transformed fibroblasts treated with 5 µM XeB for 1h in presence or absence of 5 mM n-acetylcysteine (NAC). Bar graph: P-AMPK/AMPK expressed as average fold increase over basal levels (control cells). N=3, mean ± S.E., ***p<0.001, NS: not significant (t-test).
(L) Representative Western blots of LC3 and tubulin in transformed fibroblasts treated with 5 µM XeB for 1h in presence or absence of 5 mM n-acetylcysteine (NAC). Bar graph: quantification of LC3-II/tubulin expressed as average fold increase over basal levels (control cells). N=3, mean ± S.E., ***p<0.001, NS: not significant (t-test).
(M) Normal and transformed fibroblasts were treated with 5 µM XeB in absence or presence of 5 mM n-acetylcysteine (NAC) for 24 and cell death was determined by LDH release. N=3, mean ± S.E., NS: not significant (t-test).

Figure S5. Autophagy and Cell Death, related to Figures 5 and 6.

(A) Cell cycle profile determined by flow cytometry in MCF7 cells treated with 400 µM hydroxyurea (HU) for 24h, showing percent of cells in each phase. N=3. ***p<0.001, NS: not significant.
(B) Representative Western blots of autophagy marker LC3 or tubulin as loading control in MCF10A cells treated with 5 µM XeB (1h) after a 6h incubation with 3-methyladenine (3MA). Quantification of LC3-II/tubulin expressed as fold increase over basal levels (control cells). N=3, mean ± S.E., ***p<0.001 (t-test).
(C) As in (B) using MCF7 cells. N=3, mean ± S.E., **p< 0.01, ***p<0.001 (t-test).
(D) Representative Western blots of ATG7 expression in MCF10A cells treated with a ATG7 siRNA (KD) or a scrambled siRNA (s). Bar graph: quantification of ATG7/tubulin expressed relative to control levels in cells transfected with a non-targeting scrambled siRNA (S). ATG7 protein reduced by 59 ± 12% 48 h after transfection compared with cells transfected with non-targeting siRNA. N=3, mean ± S.E., *p<0.05 (t-test).
(E) As in (D) using MCF7 cells. N=3, mean ± S.E., **p<0.01 (t-test).
(F). Determination of cell death by propidium iodide exclusion by flow cytometry in MCF10A and MCF7 cells transiently transfected with a siRNA against ATG7 for 48h. N=3, mean ± S.E., NS: not significant (t-test).
(G). Representative Western blots of caspase 3 (Casp3) and activated caspase 3 (Cleaved casp3) in normal (N) and transformed (T) fibroblasts treated either with 5 µM XeB for 24h or 2 µM staurosporine (STA) for 6h as a positive

control. Bar graph: quantification of cleaved caspase 3/tubulin expressed as average fold increase over basal levels (control cells). N=3, mean ± S.E., *p<0.05, ***p<0.001, NS: not significant (t-test).
(H) Activated caspase 3 (green) immunofluorescence in tumors treated or not with a single injection of 100 µl of 100 µM XeB 24 hrs before euthanization. N = 3. Bar: 100 µm.
(I) Left: Flow cytometry analysis of annexinV-FITC and propidium iodide (PI) staining of apoptotic cells following 5 µM XeB treatment for 24h. Right: percentage of apoptotic cells. N=3, mean ± S.E., NS: not significant (t-test).

Figure S6. Treatments Paradigm and Bioenergetics Stress in Tumors *In Vivo*, related to Figure 7.
(A) Work flow diagram of XeB treatment of tumors in mice.
(B) Top: P-AMPK immunofluorescence in tumors treated or not with a 100 µl injection of a 100 µM XeB solution 1d before euthanization. Bar: 100 µm. Bottom: P-AMPK fluorescence intensity analysis as average fold increase over basal levels (control cells). N=3, mean ± S.E., *p<0.05 (t-test).
(C) Top: LC3 immunofluorescence in tumors treated or not with a 100 µl injection of a 100 µM XeB solution 1d before euthanization. Bar: 100 µm. Bottom: LC3 fluorescence intensity analysis as average fold increase over basal levels (control cells). N=3, mean ± S.E., ***p<0.001 (t-test).

SUPPLEMENTARY VIDEOS

Supplementary Video 1, related to Figure 1. Spontaneous cytoplasmic Ca^{2+} signals in MCF10A cells.

Supplementary Video 2, related to Figure 1. Spontaneous cytoplasmic Ca^{2+} signals in MCF7 cells.

Supplementary Video 3, related to Figure 5. HeLa cells were loaded with 8 nM TMRE and then treated with 5 µM XeB at t = 0 when time lapse recording began. Images were collected every 15 min for 8 hrs with a 63X objective. Arrow shows a dividing cell. Bar: 10 µm.

SUPPLEMENTARY EXPERIMENTAL PROCEDURES

Cell Culture and Transfection

Breast cell line MCF10A was maintained in DMEM/F12 supplemented with 5% (v/v) horse serum, 10 µg/ml insulin, 20 ng/ml EGF, 100 ng/ml cholera toxin and 0.5 µg/ml hydrocortisone. T47D, PNT2 and PC3 cell lines were maintained in RPMI, MEM and Ham's F12K respectively, supplemented with 10% (v/v) FBS. MCF7, Du145 and HS578T cell lines were grown in DMEM supplemented with 10% (v/v) FBS. All cells were grown in the presence of 100 U/ml penicillin,100 µg/ml streptomycin and 0.25 µg/ ml fungizone (Gibco) at 37ºC (95%/5% air/CO_2).

Transfections of siRNA were performed with a Nucleofector® electroporator (Amaxa Biosystems). Primary human fibroblasts were transformed by high titer LZRS retrovirus driving expression of Ras^{G12V} and $Cdk4^{R24C}$ in the presence of 5 µg/ml polybrene as described (Ridky et al., 2010) and maintained in DMEM supplemented with 10% (v/v) FBS, 100 U/ ml penicillin, 100 µg/ml streptomycin and 0.25 µg/ml fungizone (Gibco) at 37ºC (95%/5% air/CO_2).

Western Blotting and Treatments

Drugs were added in fresh media as indicated in text or figure legends. Treatments were terminated by rapid removal of medium with cells on ice, followed by cell lysis with Cytobuster protein extraction reagent (Novagen) supplemented with protease and phosphatase inhibitors (complete PhosSTOP, Roche). Protein extracts were separated in 4%, 10% or 15% SDS-polyacrylamide gels and transferred to PDVF membranes (Millipore). Blocking was at room temperature for 1 h in 5% fat-free milk, and membranes were incubated overnight at 4°C with primary antibody, and then for 1 h at room temperature with a secondary antibody conjugated to horseradish peroxidase. Chemiluminescence detection used ECL-plus reagent (Pierce) and a series of timed exposures images were acquired with a FluorChem Q system (ProteinSimple) to ensure densitometric analyses were performed at exposures within the linear range. To ensure equal protein loading across gels, membranes were submerged in stripping buffer (Restore western blot stripping buffer; Pierce), incubated at 37°C for 20 min, and re-probed with a loading control antibody. Image J was used for densitometric analysis.

Microscopy

Differential contrast (DIC) and immunofluorescence imaging was performed on a Zeiss Axiovert 710 LSM ZEN confocal microscope. For time lapse microscopy, images were collected on a Nikon A1R confocal equipped with Perfect Focus in a Tokai Hit incubation chamber for 17 hours. Z-Stacks of 11 slices (1 µm intervals) were collected every 13 min. DIC and TMRE fluorescence were imaged simultaneously using a 63X plan apo lens/NA 1.4.

Calcium Signaling

Imaging of spontaneous changes in cytoplasmic Ca^{2+} concentration in MCF10A and MCF7 cells was accomplished by TIRF microscopy using a Nikon eclipse Ti inverted TIRF microscope equipped with an apo TIRF 60x, 1.49 NA lens and stage-top Tokai Hit incubator. Cells were labeled with freshly prepared Fluo-4 (5 µM) and imaged a 37°C

and 5% CO_2 at a very shallow laser angle, imaging about 100 nm into the cell. The gain on the Andor iXon EM-CCD camera was set to 300 (maximum) and images were collected every 50 ms for 2 minutes.

Oxygen Consumption

Cells were seeded in 24-well plates treated with CELL-TAK (BD Bioscience). After 24 h, cells were loaded into the machine for O_2 concentration determinations. Cells were sequentially exposed to oligomycin (1 μM), carbonylcyanide p-trifluoromethoxyphenylhydrazone (FCCP; 300 nM) and rotenone (100 nM). After each injection, OCR was measured for 5 min, the medium was mixed and again measured for 5 min. Each time point represents average of 10 different wells. Basal OCR was calculated as difference between OCR before and after oligomycin. Maximum OCR was calculated as difference between OCR after FCCP and that measured after exposure to rotenone. Data were normalized for protein concentration by lysing samples after each experiment. In preliminary studies with each cell type, three concentrations of cells were seeded. Linear relationships between OCR and number of cells seeded were observed. The cell number was chosen that provided a nearly confluent uniform monolayer of cells. Before and at the end of each experiment, uniformity of the monolayer was evaluated by DIC microscopy.

Clonogenic Assay

Briefly, MCF7, T47D and PC3 cells were treated with 5 μM XeB for 24 h and then the population of cells that remained attached were trypsinized and counted. Then, one thousand cells were seeded and left undisturbed for 1 wk. Finally, colonies obtained were fixed and stained with 6% glutaraldehyde and 0.5% crystal violet, analyzed and counted.

Growth Curves

Breast, prostate and human fibroblast cells were plated in growth media at a density of 50,000 cells per well. Cells were counted each day using a Beckman Coulter Multisizer 4. Growth curves were performed independently at least three times.

Cell Cycle Analysis

Cells were cultured in 24 well plates (10^5 cells/well) and treated or not with 5 μM XeB for 24 h. Cells were harvested, washed in PBS, permeabilized with methanol and re-suspended in 1 ml of 0.1% sodium citrate containing

0.05 mg of Propidium iodide and 50 µg of RNase for 30 min at room temperature in the dark. Flow cytometry was performed on FACS Canto (BD Biosciences), and collection and analyses of data were performed using CellQuest Software (BD Biosciences).

Apoptosis Assessed by Flow Cytometry

After 24h of treatment, cells were harvested, and Annexin V-FITC was added to a final concentration of 2.5 µg/ml. PI was added at a concentration of 2 µg/ml. The Annexin V-FITC and PI-labeled cells were analyzed by FACS (FACS Canto, BD Biosciences, San Jose, CA, USA).